Departamento de Bioingeniería e Ingeniería Aeroespacial

TRABAJO FIN DE GRADO

ACCURACY OF THE ATTENUATION CORRECTION ON SMALL-ANIMAL PET/CT

Autor: Irene Mayorga Ruiz

Co-Directores: Juan José Vaquero López

Verónica García Vázquez

Leganés, 9 de julio de 2015

Título: Accuracy of the attenuation correction on small-animal PET/CT
Autor: Irene Mayorga Ruiz
Director: Juan José Vaquero López
Co-director: Verónica García Vázquez

EL TRIBUNAL

Presidente:

Vocal:

Secretario:

Realizado el acto de defensa y lectura del Trabajo Fin de Grado el día 9 de julio de 2015, en la Escuela Politécnica Superior de la Universidad Carlos III de Madrid, acuerda otorgarle la CALIFICACIÓN de:

VOCAL

SECRETARIO PRESIDENTE

AGRADECIMIENTOS

Quiero dar las gracias a todas aquellas personas: profesores, técnicos, compañeros amigos y familiares que durante estos cuatro años han hecho posible haber llegado a este punto gracias a su apoyo, ilusión y confianza.

A Manuel Desco, por darme la oportunidad de realizar mi trabajo de fin de grado en el LIM, permitiéndome así conocer la realidad de la investigación así como a personas maravillosas que desde el primer día me acogieron con los brazos abiertos.

A Juan José Vaquero y Verónica García darles las gracias por ser tan pacientes y ayudarme en todo lo posible durante la realización de este trabajo. En especial debo agradecer a Verónica García su entrega y disposición a ayudarme en todo momento y siempre con una sonrisa. Gracias por tu infinita paciencia. Este trabajo es tan tuyo como mío.

Por último, darle las gracias a mis padres y hermana por dejar equivocarme y rectificar pudiendo así encontrar mi camino. Gracias por el apoyo incondicional que durante estos cuatro años, y en especial en el primero, me habéis dado, empujándome así a continuar y no abandonar.

INDEX of CONTENTS

INDEX of FIGURES

INDEX of TABLES

ACRONYMS

AC: Attenuation corrected

Bq: Becquerel

Ci: Curie

cps: Counts per second (image units)

CT: Computed tomography

EM: Expectation maximization

FBP: Filtered back projection

FDG: 2-deoxy-2-(18F) fluoro-D-glucose

FDK: Feldkamp-Davis-Kress (CT reconstruction algorithm)

FOV: Field of view

F-18: Fluorine-18

Ga-68: Galium-68

Ge-68: Germanium-68

HU: Hounsfield units

IDL: Interactive data language

LOR: Line of response

ML-EM: Maximum-likelihood expectation maximization

MMWKS: Multimodality workstation

MRI: Magnetic resonance imaging

NAC: Non-attenuation corrected

Na-22: Sodium-22

OSEM: Ordered-subset expectation maximization

PET: Positron emission tomography

RC: Recovery coefficient (according to NEMA protocol)

RC2: Recovery coefficient (according to usual quantification protocol)

SI: International system of units

SNR: Signal to noise ratio

SPECT: Single-photon emission computed tomography

STD: Standard deviation

US: Ultrasound

VOI: Volume of interest

2D: Two-dimensional

3D: Three-dimensional

4D: Four-dimensional

ABSTRACT

Positron emission tomography (PET) is a functional medical imaging modality that is acquired after the administration of a radiotracer. PET imaging technique is based on the coincident detection of gamma photons of 511 keV. If any of the antiparallel gamma photons does not reach the PET detectors due to attenuation (scatter or absorption), a coincidence is not recorded, which means missing information. Attenuation is the largest correction that is applied to PET images in order to obtain an accurate quantification of radiotracer activity concentration. One approach to perform that correction is based on creating an attenuation map using a computed tomography (CT) image in which its Hounsfield units are transformed into attenuation coefficients at 511 keV by applying a bilinear approximation. Then, the attenuation map is used to correct PET data in the reconstruction process.

There are no studies that compare non-attenuation corrected PET images and attenuation corrected PET images acquired with the Argus PET/CT scanner with different energy windows and reconstruction methods from a practical point of view (quantification results). The aim of this study was to perform that comparison by means of three different experiments.

Our results showed that attenuation correction has an impact on the image data and results are different depending on the Argus PET/CT reconstruction method and energy window used. For filtered back projection (FBP) and ordered –subset expectation maximization (OSEM) 2D reconstruction methods, image activity (counts per second) increases when applying the attenuation correction independently of the attenuation medium and the energy window. However, for OSEM 3D, the activity decreases. The absolute relative error between the estimated and real activity concentration either for non-attenuation corrected PET images or attenuation corrected PET images was smaller than 5%. Finally, recovery coefficients for non-attenuation corrected PET images are similar than the ones for attenuation corrected PET images. The segmentation rule does not

affect the recovery coefficient calculation. However, when segmenting small objects, VOI mean value does not provide an accurate activity concentration.

Keywords: Positron emission tomography (PET), PET/CT scanner, Attenuation correction, and Recovery coefficient.

1. INTRODUCTION

This section presents a basic background about medical imaging, focusing on PET/CT imaging techniques.

1.1 Medical imaging

Medical imaging refers to non-invasive techniques that produce images of body tissues to assist diagnosis or treatment of different medical conditions.

Medical imaging techniques can be divided into two groups depending on the information that provides:

- Structural: Techniques that provide images with anatomical information. Some examples of structural imaging modalities are X-ray, computed tomography (CT) (Figure 1) and structural magnetic resonance imaging (MRI). X-ray and CT use electromagnetic ionizing radiation, which means that work with photons that have enough energy to produce ion pairs by interaction with matter. MRI is a non-ionizing radiation technique that is based on the resonant frequency of protons (H+).

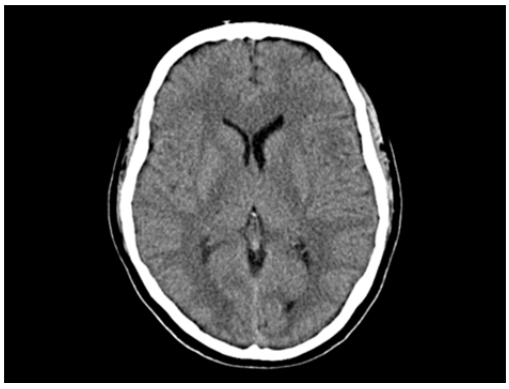

Figure 1. Brain CT image

- Functional: Techniques that provide images with physiological information. Some functional imaging modalities are functional MRI (fMRI), contrast-enhanced CT or nuclear medicine imaging techniques such as position emission tomography (PET) (Figure 2) and single-photon emission computed tomography (SPECT).

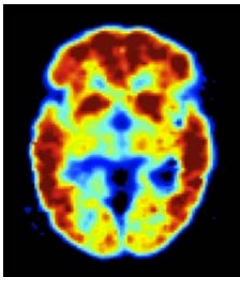

Figure 2. Brain PET image

Both types of medical imaging can be combined forming systems able to provide structural and functional information of the body. Nowadays, multimodal medical imaging scanners (e.g. PET/CT, SPECT/CT or PET/MRI -Figure 3-) are widely used not only because more information is provided, but also because, as both functional and anatomical images are acquired in the same scanner, images are intrinsically registered (i.e. images are in spatial concordance).

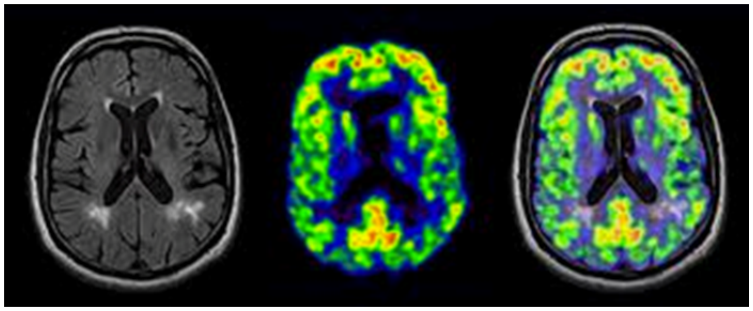

Figure 3. Comparative between MRI, PET and PET/MRI images. Brain MR image (left), brain PET image (middle) and brain PET image superimpose on the MR image (right)

Medical images can also be classified according to their number of dimensions:

- Planar: Images that provide two-dimensional (2D) information such as ultrasound (US) images, X-ray and 2D images acquired using optic techniques.
- Tomographic: Images that provide three-dimensional (3D) information so that an entire volume is acquired. Some examples are CT, MRI and PET images.
- Dynamic: Images that provide four-dimensional (4D) information so that an entire volume is acquired at different times. Some examples are dynamic PET and SPECT images.

Images are shown using a standardized way called anatomical body planes. The three basic body planes are coronal (yz plane), sagittal (xz plane) and axial (xy plane) planes (Figure 4).

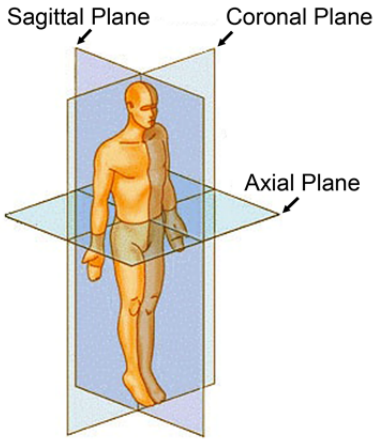

Figure 4. Scheme of anatomical body planes

1.2 Multimodality workstation

All PET/CT image acquisitions, reconstructions and processing (registration and quantification) in this bachelor thesis were performed using the multimodality workstation (MMWKS, Figure 5). This software was implemented by Laboratorio de Imagen Médica (Hospital General Universitario Gregorio Marañón, Madrid) in interactive data language (IDL) programming language [1]. MMWKS is a user-friendly interface of the multimodal Argus PET/CT scanner (Sedecal) for small animals (Figure 6).

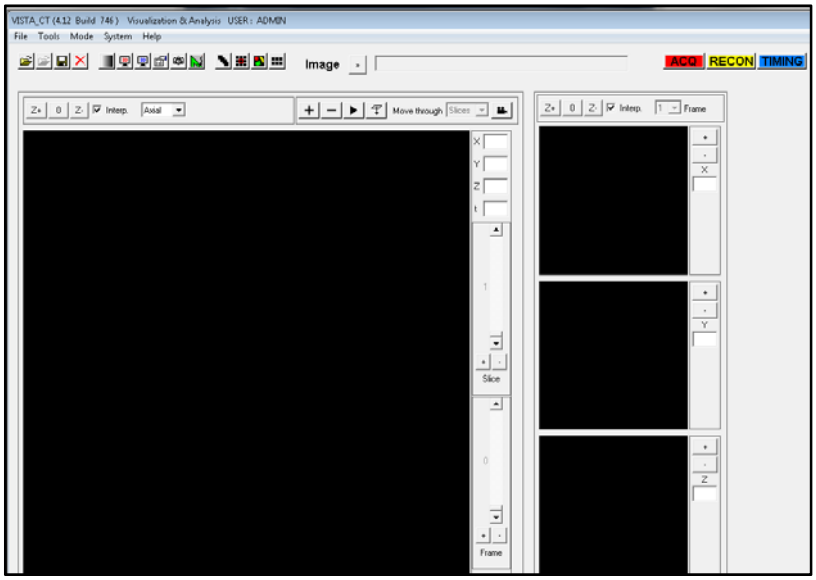

Figure 5. MMWKS software

Figure 6. Argus PET/CT scanner

1.3 Computed tomography

Computed tomography (CT) is a diagnostic medical imaging technique that is based on the attenuation of the X-rays to create a tomographic image.

The CT scanner consists on a source of X-rays that rotates around the subject and a detector panel that also rotates in order to be always placed diametrically opposite to the X-rays beam (Figure 7). The X-rays beam passes through the subject and, depending on the tissue density, X-rays photons will be absorbed by the tissue (attenuated) and will not reach the detector. The two principles processes of photon absorption are the photoelectric effect and the Compton effect. In the first process, a photon interacts with a tightly bound electron. The photon transfers practically all of its energy to the electron and ceases to exist. In Compton process (incoherent scatter), a photon interacts with an electron that is not tightly bound to the atom. Both the photon and electron are scattered [2].

2D images or projections are acquired while rotating both the x-rays source and the detector. Then, a 3D volume is reconstructed from these projections. Finally, attenuation coefficients are transformed to Hounsfield units (HU) scale where x-ray attenuation of distilled water is defined as 0 HU and attenuation of air as -1000 HU at standard pressure and temperature.

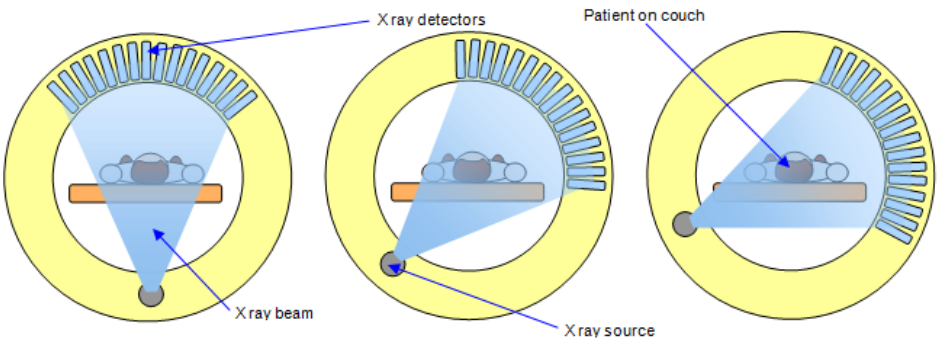

Figure 7. CT scanner (X-ray source and detectors)

1.4 Positron emission tomography

Positron emission tomography (PET) is a functional tomographic medical imaging technique [3]. PET and SPECT are the two most common imaging modalities in nuclear medicine. Nuclear imaging uses low doses of radioactive isotopes linked to compounds that are used by the body's cells.

1.4.1 Radioactive isotopes

Radioactive isotopes or radioisotopes are isotopes that have unstable nuclei and lose energy by emitting ionizing radiation. There are radioactive isotopes that can be found in the nature such as carbon-14 and others that are produced artificially, for example, in nuclear reactors and cyclotrons.

The radioactive isotope is bond to a biological substance that not only makes the complex biocompatible but also sets its biodistribution. These characteristics allow the control and the specialization of the radiotracer or radiopharmaceutical (radioactive isotope + biological substance) for each disease diagnosis. Figure 8 shows an example of one of the most used radiotracer in diagnosis, 2-deoxy-2-(18F) fluoro-D-glucose (FDG). This radiopharmaceutical is formed by a glucose support molecule (biological substance) and Fluorine-18 (F-18) radioisotope. It is widely used in PET studies because FDG allows the visualization of glucose metabolism. This feature is very important for cancer diagnosis as far as cancer cells have more glucose metabolic consumption than healthy cells.

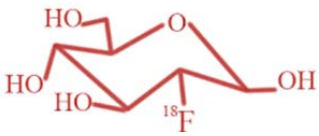

Figure 8. FDG radiopharmaceutical

The activity of the radiotracers decays exponentially according to the half-life of the radioisotope, i.e. the time that takes to the radioisotope to lose the 50% of its

activity. The radioisotope activity (A) can be calculated by using the following equation that takes into account its initial activity (A_0), the time passed since its production (Δt) on the cyclotron or radioisotope generator, and its half-life ($T_{1/2}$) [4].

$$A = A_0 \cdot e^{-\frac{\ln 2}{T_{1/2}}\Delta t}$$

1.4.2 PET image acquisition

PET image is acquired after the administration of a radiotracer that decays emitting positrons. This radiopharmaceutical is concentrated specifically in some organs or tumours depending on its biological substance. Those emitting positrons interact with the electrons of the matter and, by a process called annihilation, produce two antiparallel gamma photons of 511 keV per annihilation. PET imaging technique is based on the coincident detection of those two 511 keV gamma photons.

If two gamma photons are simultaneously detected by two small detectors, a coincidence event is recorded. It can be inferred that the annihilation must have occurred along the line connecting those detectors or line of response (LOR). To increase the sensitivity of the scanner, the patient is surrounded by a ring of small detectors rather than only two. The LOR is characterized by the angle of orientation of the LOR (θ) and the shortest distance between the LOR and the centre of the gantry (r). Coincidence events can be recorded as a sinogram. Each pixel of a sinogram (polar coordinates r and θ) represents a LOR and its pixel value, the number of coincidence events detected by the two detectors along that LOR. A horizontal line in the sinogram is called a projection and takes into account all LORs at a given angle. Finally, PET image is reconstructed based on sinograms (one sinogram per slice across all angles). Figure 9 shows the process that takes place for PET image acquisition.

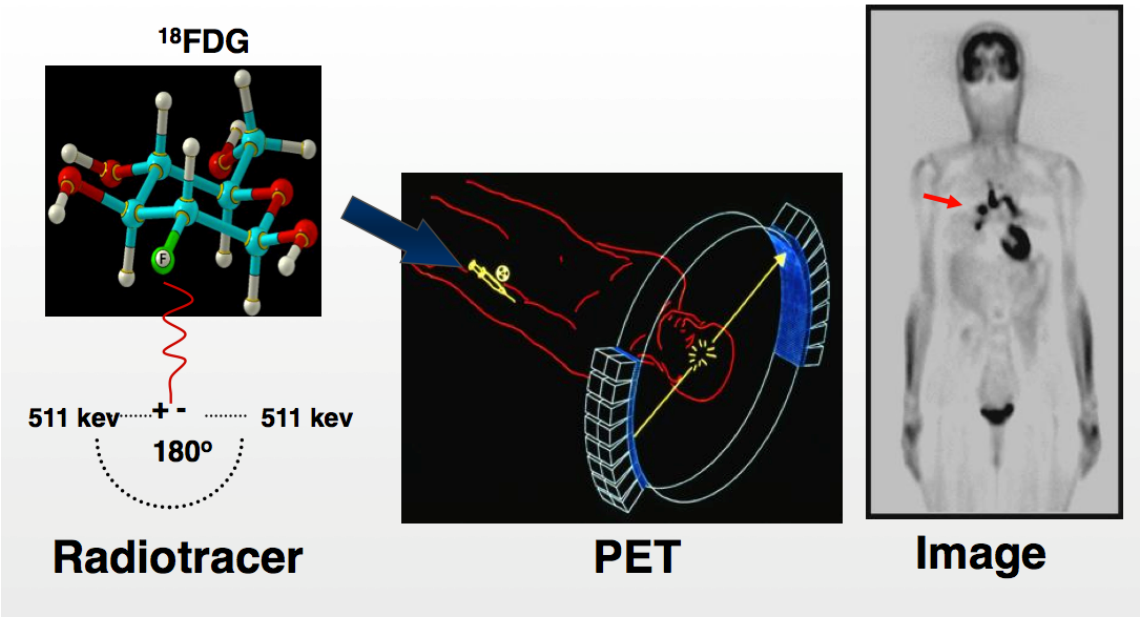

Figure 9. Scheme of PET image acquisition. Radiotracer and annihilation (left). PET scanner scheme and ring of detectors (middle) and PET image (right). Image courtesy of Dr. John C. Clark, University of Cambridge

1.4.3 PET reconstruction

Figure 10 shows the classification of image reconstruction methods [4]. There are two main groups of algorithms:

- Analytical methods: Methods that offer a direct mathematical solution (exact solution to a system of equations) for the reconstruction of an image.

- Iterative methods: These methods basically involve estimating image bio-distribution and comparing the sinogram obtained from this estimate to the measured sinogram. The iterations continue until there is a convergence between the estimated and the measured sinogram. These algorithms are computationally more intense than analytical methods.

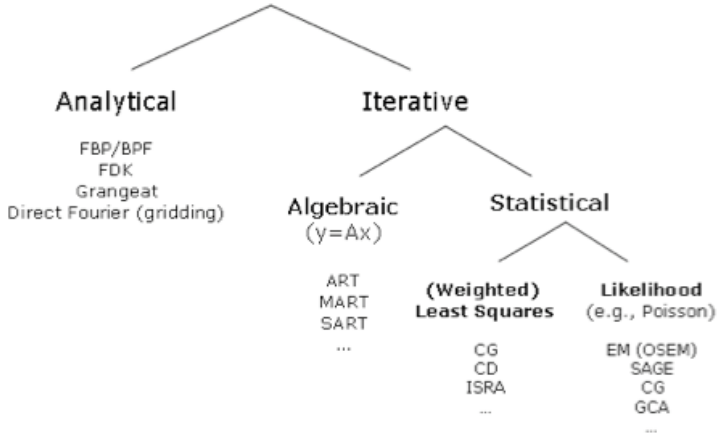

Figure 10. Classification of image reconstruction algorithms

Since FBP (analytic) and OSEM (iterative) algorithms were used in this bachelor thesis, the basics of these reconstruction methods are explained in the following sections.

Compared to CT and MRI, PET images appear much blurrier and/or noisier, due to the relatively limited number of photons that can be collected during an imaging study. In addition, detector resolution is poorer due to the detector physics. Therefore, PET image quality is affected by partial volume effect (loss in apparent activity in small objects or regions because of the limited resolution of the scanner). However, PET modality could have very high sensitivity and specificity depending on the tracer used.

Filtered Back Projection

The most known analytical algorithm is filtered back projection (FBP). This method is based on the projection slice theorem or central section theorem [5] that states that:

The **Fourier transform** *of the* **projection** *at angle θ is equal to the two-dimensional Fourier transform of the object, evaluated in the direction θ in Fourier transform space.*

2D-FBP involves two principal steps: filtering the projection data and then back projecting the filtered data along the angle used for the application of the Projection Slice Theorem to create the reconstructed image. Filtering the projection data is used in order to eliminate blurring appeared during the back projection due to the oversampling in the centre of the Fourier space. Analytical methods usually use the ramp filter because it accentuates the edge values and reduce the values at the centre of the Fourier space.

MMWKS interface shows the following parameters in FBP reconstruction:

i) Span: Degree of axial angular compression of LORs (always 3).

ii) Dmax: The maximum number of rings (between 13 and 30) allowed being in coincidence with one another. Higher number result in axial blurring of objects. Default value is 16.

iii) Filter: Three different filters can be used [6]:

- Ramp filter (default): This filter gives priority to high frequencies components to provide the best spatial resolution on high count images (alpha = 1.0 and cut-off = 1.0).
- Hann filter: This method filters high frequencies and improves the signal to noise ratio (SNR) in spite of losing resolution and contrast quality (alpha =1.0 and cut-off =0.5). Appropriate to work with low count images.
- General (Butterworth) filter: The user can define if the high frequencies are filtered or if the SNR is improved by adjusting the alpha and cut-off parameters (alpha = 0.5-1.0, cut-off = 0-1.0).

2D-FBP reconstruction is easy to implement and a fast method. However, it results in poor image quality (streak artifacts and low SNR) in case of poor count rates (short scan time or low activity). Iterative reconstruction algorithms can be used to overcome these limitations.

Ordered- subset expectation maximization

Ordered–subset expectation maximization (OSEM) iterative method is based on the expectation maximization (EM) algorithm. EM iterates by alternating between an expectation (E) step and a maximization (M) steps. The E-step computes the expectation of the complete-data log likelihood function conditioned on the current estimate of the image and the M-step estimates the unknown image, which maximizes that expectation function. The OSEM method is a modification of the EM algorithm, which divides the LOR data in different disjoint subsets. Those subsets are iterated independently one from another reducing the reconstruction time.

Two different OSEM reconstruction methods (OSEM 2D and OSEM 3D) were used in this bachelor thesis. In OSEM 2D, each slice is reconstructed independently and then all slices are put together to reconstruct the whole volume, while OSEM 3D works directly on the volume acquired [7].

MMWKS interface shows the following parameters in OSEM 2D reconstruction:

i) Span: Degree of axial angular compression of LORs.

ii) Dmax: The maximum number of rings (between 13 and 30) allowed being in coincidence with one another. Higher number result in axial blurring of objects. Default value is 16.

iii) Iterations: Number of repetitions of the EM algorithm (between 1 and 99).

iv) Subsets: Number of subsets (between 1 and 8). The smaller the subset dimensions, the higher the resolution.

In the case of OSEM 3D, the user only can select the number of iterations and the number of subsets.

The major limitation of these methods is that they do not converge to a stable solution. The general practice is to terminate these methods early by reducing the number of iterations to limit noise amplification caused by overfitting.

1.4.4 PET image corrections

Once both generated antiparallel gamma photons reach the detector at the same time a true coincidence is recorded (Figure 11). However, there are other types of coincidences that take place in PET acquisition such as random and scattered coincidences. Moreover, gamma photons can be absorbed by the body or scattered and do not reach the detector (attenuation). In order to obtain an accurate quantification of radiotracer activity concentration, these factors (in rough order of decreasing magnitude: attenuation, scattered coincidences and random coincidences) must be taken into account.

Random coincidences

A random coincidence occurs when two photons coming from different annihilation process reach the detectors within the same time-window and is registered as a coincidence (Figure 11). Random coincidences reduce image contrast since the system cannot identify them and therefore they are included in the image reconstruction process. The correction is based on the estimation of these random coincidences and they are subtracted from the measured data in each LOR.

Scattered coincidences

A scattered coincidence occurs when one or both gamma photons undergoes scatter (photon is deflected and its energy decreases) prior to detection. Since the direction of the photon is changed, it is highly likely that the resulting coincidence will be assigned to a wrong LOR (Figure 11). Scatter reduces image contrast and adds noise. As in the case of random coincidences, the correction of the scatter coincidences is based on estimating them and they are subtracted from the measured data.

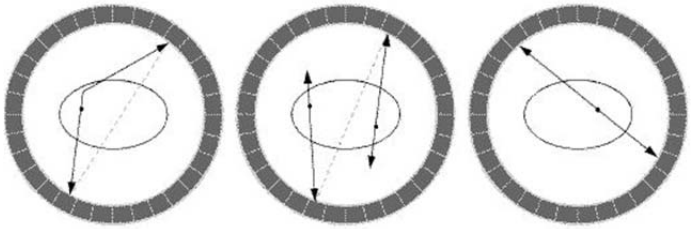

Figure 11. Types of coincidences. Scatter coincidence (left), random coincidence (middle) and true coincidence (right)

Attenuation

Gamma photons can be absorbed by the body. If any of the antiparallel gamma photons does not reach the detectors due to attenuation (absorption or scatter), a coincidence is not recorded, which means missing information (Figure 12). The longer the path of the photon in the tissue, the higher the likelihood of being absorbed or scattered.

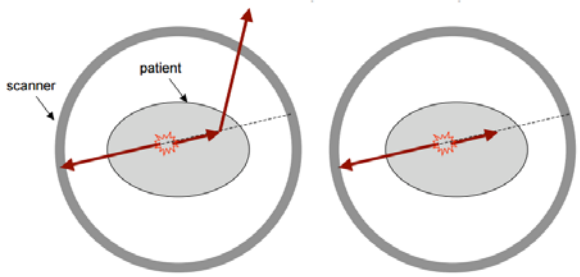

Figure 12. Attenuation. Loss of coincidence events through photon scattered out of the field of view (left) or photon absorption (right)

Figure 13 shows the attenuation artifact: There is high activity toward the surface and relatively low activity toward the centre. This is due to photons that originate from structures deeper in the body are more highly attenuated by the intervening soft tissue than those originating closer to the surface.

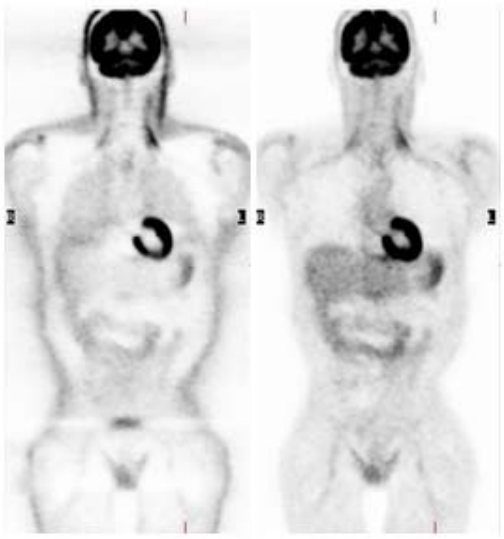

Figure 13. Attenuation artifact on PET image. Non-attenuation corrected PET image (left) and attenuation corrected PET image (right).
Source: http://www.med.harvard.edu/JPNM/chetan/petct/petct.html

There are several methods to correct attenuation in PET, but all of them uses transmission images either with PET or CT scanner to obtain tissue properties [7-10]:

- PET transmission images: Source is gamma-emitter radioisotopes. The most common approach is to use a long-lived rod positron emitter source (e.g. Germanium-68, Ge-68) that rotates around the scanner. The transmission scan is acquired with the patient positioned in the scanner. One approach is to acquire the transmission scan post injection immediately after the emission scan without moving the patient from the bed. Although the residual activity is present from the radiotracer injection, its value along an LOR is small. However, the detectors must be sufficiently efficient to detect both transmission and emission activities. Moreover, conventional PET transmission scan takes about 20 minutes (more than a CT scan) to acquire enough counts for good accuracy of the measured attenuation correction factors.

- CT transmission images: Source is X-rays. CT-based attenuation correction consists on the correction of PET image data with attenuation coefficients

extracted from a CT image acquired on the same scanner (PET/CT devices). CT intensity values represent the x-ray attenuation coefficients of body tissues in Hounsfield units (HU) scale. The x-ray source in CT emits photons with a broad energy spectrum from 40 keV to 140 keV. The key point of this attenuation correction method is the transformation of x-ray attenuation coefficients into PET attenuation coefficients (photons of 511 keV) as attenuation is affected by photon energy. There are several methods to perform this transformation, from a simple linear transformation to more complex transformations.

In MMWKS, PET images can be reconstruction with CT-based attenuation correction ([10]). The procedure followed by MMWKS is the creation of an attenuation map using the CT image in which HU are transformed into attenuation coefficients at 511 keV by applying a bilinear approximation (Figure 14). That attenuation map has the dimensions and voxel size of the corresponding PET image and both images are registered, which means spatial concordance between corresponding attenuation map and PET image. Then, the attenuation map is forward projected in order to combine that information with PET data. Finally, attenuation corrected PET data is reconstructed in order to obtain the attenuation corrected PET image (Figure 15).

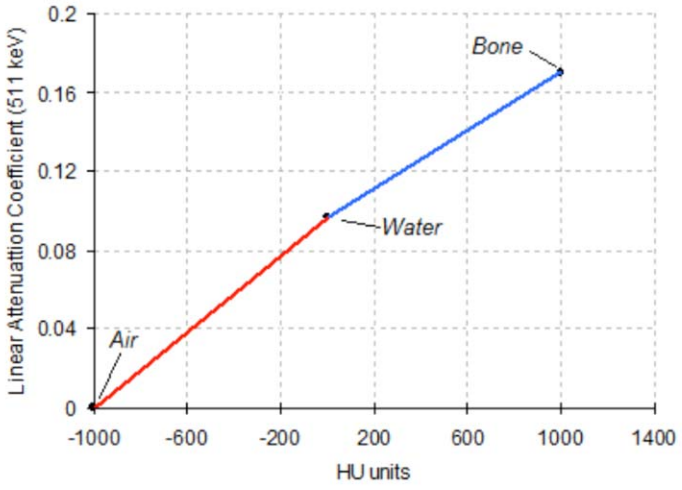

Figure 14. Transformation of HU into attenuation coefficients at 511 keV

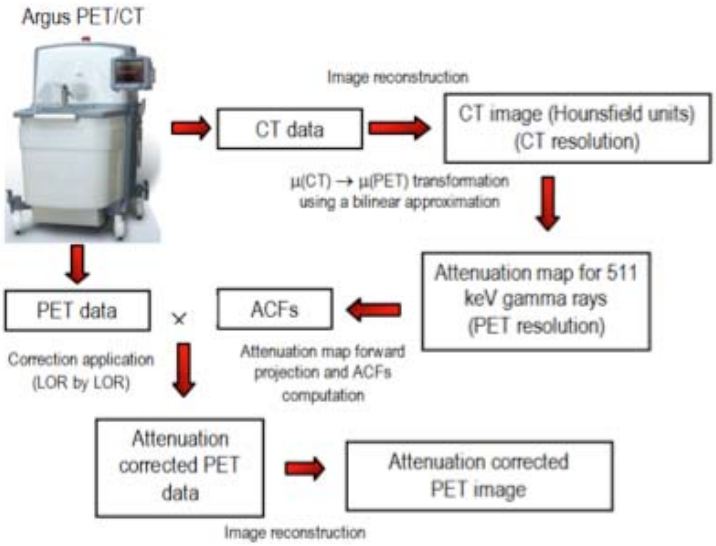

Figure 15. CT-based attenuation correction workflow

PET activity data correction

PET scanner records detected coincidences. The activity in PET images is expressed in counts per second (cps). It is preferred to have these data, for instance, in Becquerels (Bq). A Bq is the activity of a radioactive material in which one-nucleus decays per second (the radioactivity unit of the international system of units –SI-). This transformation is performed by applying a calibration factor that relates, for instance, activity in Bq and cps. This value depends on radioisotope, PET scanner, image acquisition, reconstruction method and applied corrections.

The procedure followed in Laboratorio de Imagen Médica to calculate the calibration factor is shown in Figure 16. A homogeneous dilution of a specific radiopharmaceutical (≈400 μCi) and water is used to fill an Eppendorf (1 ml = 1 cc) with a pipette and a syringe (40 ml, diameter 30 mm). The Curie (Ci) is a non SI-unit of radioactivity and is defined as 3.7×10^{10} decays per second (roughly the activity of 1 gram of Radium-226). The activity of the Eppendorf is measured using a well counter or dosimeter. The activity measurement is performed three times in order to average the values obtained and get an accurate value. The syringe is acquired with the PET scanner. If PET images are attenuation corrected, a CT

image of the syringe must also be acquired. Once the PET image is reconstructed, a cylindrical volume of interest (VOI) of radius 8 mm and height 8.5 mm (1.7 cc) centred on the syringe is segmented on the PET image. Finally, the calibration factor (Bq/cps) is obtained by dividing the Eppendorf activity concentration (Bq/cc) by the mean value of the PET VOI divided by its volume in cc (cps/cc).

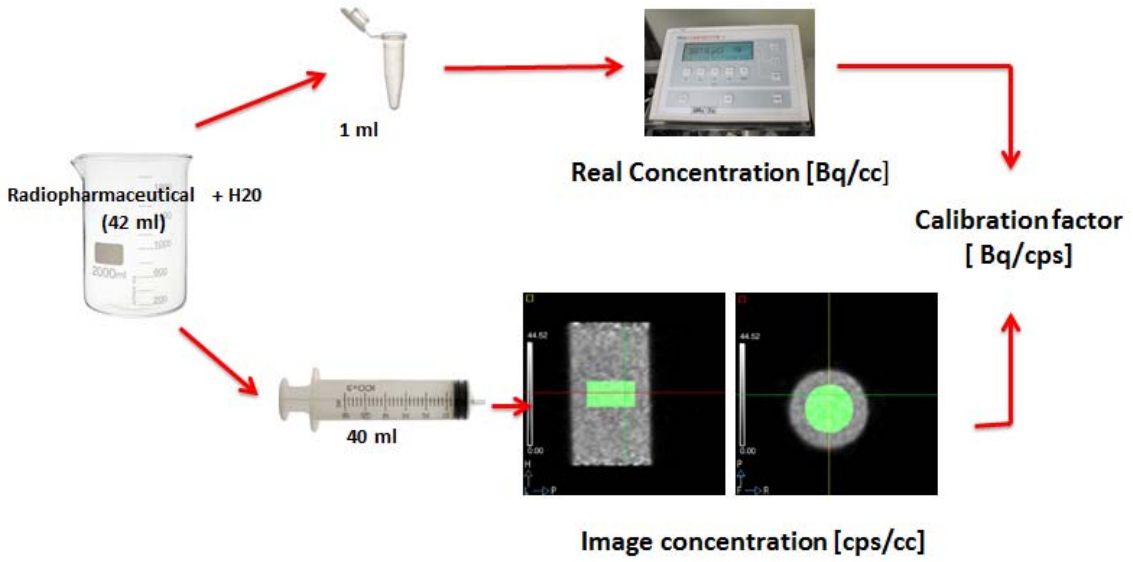

Figure 16. Calibration factor protocol. Segmented VOI (green) superimposed on the corresponding PET image

2. MOTIVATION and OBJECTIVES

Attenuation is the largest correction applied to PET images in order to obtain an accurate quantification of radiotracer activity concentration. PET images provide crucial functional information and attenuation correction is important from the diagnostic point of view.

There are studies that have evaluated the attenuation correction on PET images acquired with preclinical PET/CT scanners. In [11], the authors evaluated the difference between non-attenuation corrected PET images and attenuation corrected PET images acquired with a microPET R4 system (Concorde Microsystems/Siemens) scanner using an energy window of 350–650 keV and FBP, OSEM 2D and OSEM 3D reconstruction methods. This evaluation was based on uniformity (measurement of statistical noise in both hot and cold regions), recovery coefficient (gives information of the minimum object size to get reliable data) and spillover ratio (an indication of the spatial resolution). The attenuation correction method was either using a PET transmission scan (Ge-68 line source) or using a CT acquired with Discovery ST PET/CT (General Electric) clinical system. A registration step was necessary in order to align PET/CT images. HU were converted to linear attenuation coefficients at 511 keV. In [12], the authors assessed the difference between a quadratic and a bilinear approximation in the CT-based attenuation correction using a FLEX Triumph PET/CT scanner (Gamma Medica-Ideas). For soft tissues, both methods give similar results but, for bones, the quadratic approach produced slightly enhanced increment of PET activity concentration than the bilinear approximation. The energy window was 250–700 keV and the reconstruction method was OSEM 2D. In [10], the authors evaluated the implementation of the CT-based attenuation correction (bilinear approximation) in the Argus PET/CT scanner (Sedecal). The evaluation was performed by using χ^2 parameter that measures the difference between the acquired data (all LORs) and the estimated data obtained from the reconstructed image (OSEM 3D) and comparing the profiles of non-attenuation corrected images and corrected images. The results showed better results when using attenuation

corrected PET images. On the other hand, in [13] the authors compared the spillover ratio and image noise in air and water for non-attenuation corrected PET images and attenuation corrected PET images acquired with an Argus PET/CT. The comparison was performed for different reconstruction methods (FBP and OSEM 2D) for Galium-68 (Ga-68) PET images with a 400-700 keV energy window. However, there are no studies that compare non-attenuation corrected PET images and attenuation corrected PET images acquired with this scanner with different energy windows and reconstruction methods. The aim of this study was performed that comparison regarding a practical point of view (quantification results).

The objectives to be achieved in this bachelor thesis were

1. To quantify the accuracy of the attenuation correction on PET images after attenuation correction.

2. To measure the accuracy of the activity concentration measured in PET images after applying the attenuation correction.

3. To quantify the effect of applying the attenuation correction on the recovery coefficient.

on a small-animal Argus PET/CT scanner. The evaluation was performed changing the energy window (100-700 keV, 250-700 keV and 400-700 keV) and the reconstruction method (FBP, OSEM 2D and OSEM 3D).

3. MATERIALS and METHODS

This section describes the different experiments that were performed on the Argus PET/CT scanner to achieve the following goals:

1. To quantify the accuracy of the attenuation correction on PET images.
2. To measure the accuracy of the activity concentration measured in PET images after applying the attenuation correction.
3. To quantify the effect of applying the attenuation correction on the recovery coefficient.

3.1 STUDY I: Accuracy of the attenuation correction on PET studies

The aim of this study was to quantify the effect of applying the CT-based attenuation correction on PET studies and the accuracy of the attenuation correction. The phantom used in this experiment simulated a small animal, namely a mouse, with a region of high activity (e.g. a tumour). At first, the volume inside the phantom was filled with air to simulate a non-attenuating medium but afterwards, it was filled with water to simulate soft tissue. Apart from studying the effect of the medium, attenuation correction was evaluated in images acquired with different energy windows and reconstructed with different methods.

3.1.1 Phantom characteristics

The phantom used in this study was composed by a radioactive point source of Sodium-22 (Na-22) placed inside a universal sample tube (70 mm height and 30 mm diameter) (Figure 17). Table 1 shows some details of the radioactive source. In accordance with the half-life of Na-22, the activity of the radioactive source remained almost unchanged during the whole experiment. The universal

sample tube was filled with either air to simulate a non-attenuating medium or water to simulate soft tissue.

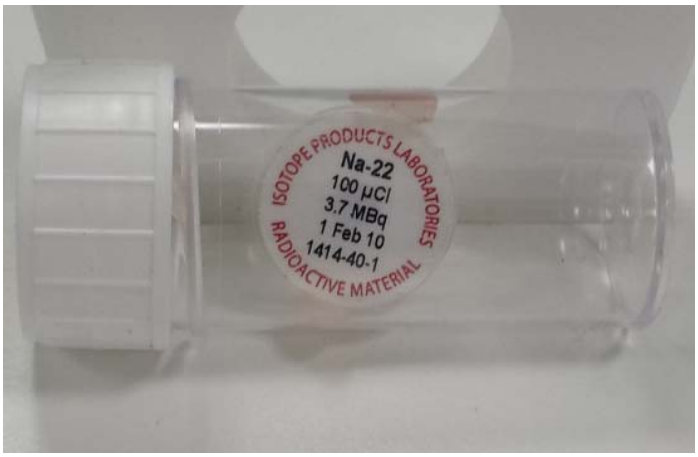

Figure 17. Phantom (Study I)

Isotope	**Na-22**
Physical dimensions [mm]	**ϕ 1.92 x 3.24 height**
Half- life [years]	**2.906**
Initial activity (1 Feb. 2010) [uCi]	**100**
Study initial activity (10 Dec. 2014) [uCi]	**≈ 27.44**

Table 1. Na-22 radioisotope characteristics (Study I)

3.1.2 Image acquisition protocol

Two different PET/CT studies were acquired on the Argus PET/CT scanner using the MMWKS, one for air medium and other one for water medium.

CT acquisition

The CT image of the phantom with the air medium was used to obtain the attenuation map that was applied to the PET image of that phantom for attenuation correction. A similar process was performed with the water phantom as the medium changes the attenuation and therefore the attenuation map.

CT images were acquired using the default parameters set by the Argus PET/CT system with the exception of the voltage and the current. Table 2 shows the CT protocol, and Figure 18 and Figure 19 the scout images of the air and water phantom respectively. Scout images are coronal and sagittal X-rays projections where the user can select the acquisition field of view (FOV).

Projections	**360**
Binning	**4**
Frames	**8**
Voltage [kV]	**40**
Current [uA]	**≈ 340**
Acquisition time [min]	**10**

Table 2. CT protocol (Study I)

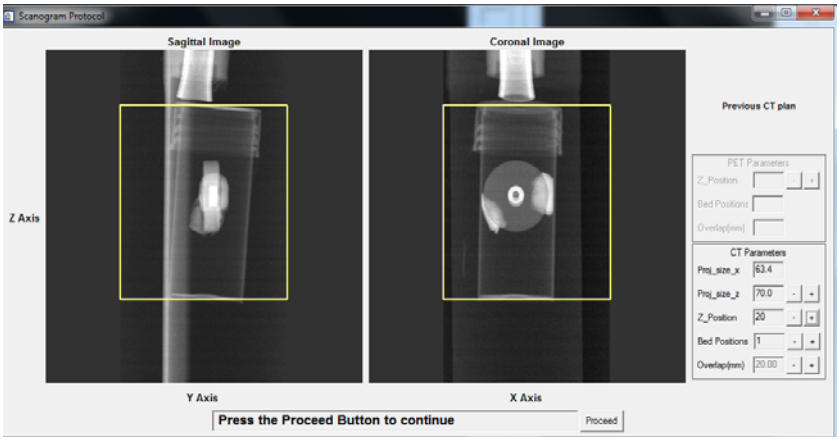

Figure 18. Scout images of air phantom (Study I). Yellow rectangles show the CT acquisition FOV

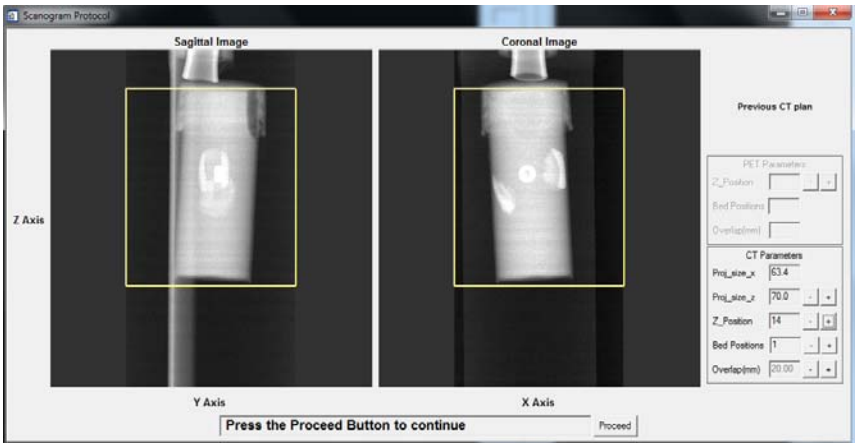

Figure 19. Scout images of water phantom (Study I). Yellow rectangles show the CT acquisition FOV

PET acquisition

Three PET images were acquired of every phantom setting the same scan time and radioisotope but a different energy window. Table 3, Figure 20 and Figure 21 shows the PET protocol and the acquisition FOV of the air and water phantom respectively.

Energy window [keV]	**(100-700), (250-700), (400-700)**
Protocol	**Static (Emission Scan)**
Acquisition time [min]	**20**

Table 3. PET acquisition protocol (Study I)

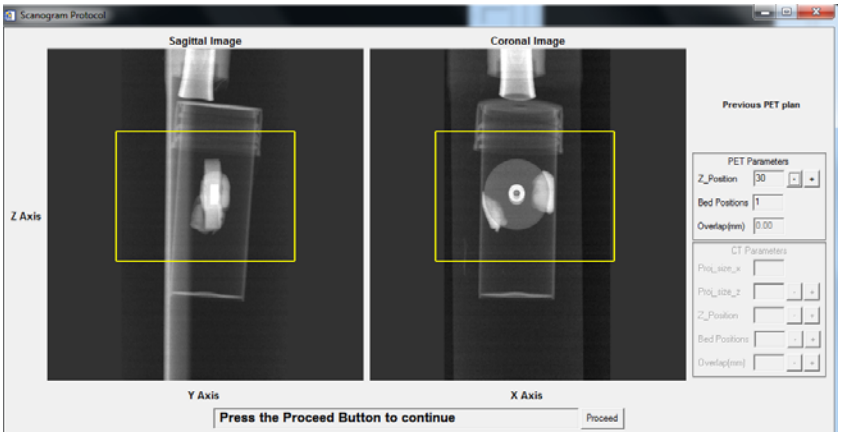

Figure 20. PET acquisition FOV of air phantom (Study I).Yellow rectangles show the acquired volume

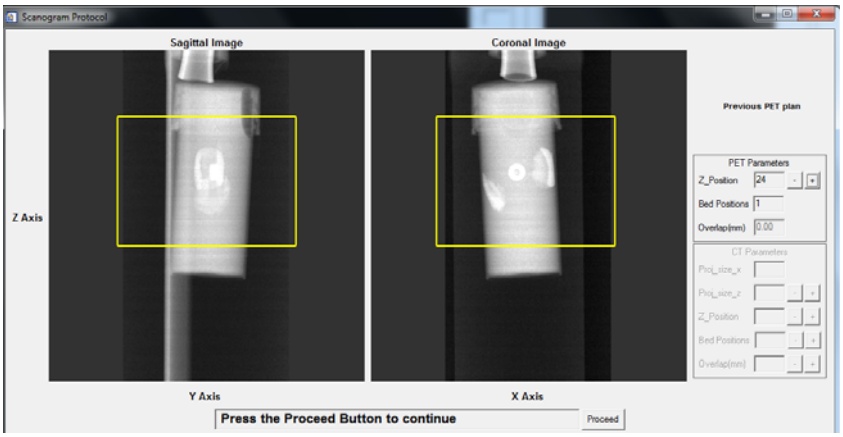

Figure 21. PET acquisition FOV of water phantom (Study I). Yellow rectangles show the acquired volume

3.1.3 Image reconstruction

CT reconstruction

CT images were reconstructed using the Feldkamp-Davis-Kress (FDK) algorithm implemented in MMWKS (Figure 22). FDK method is based on an approximation of the 2D FBP algorithm for cone-beam geometry.

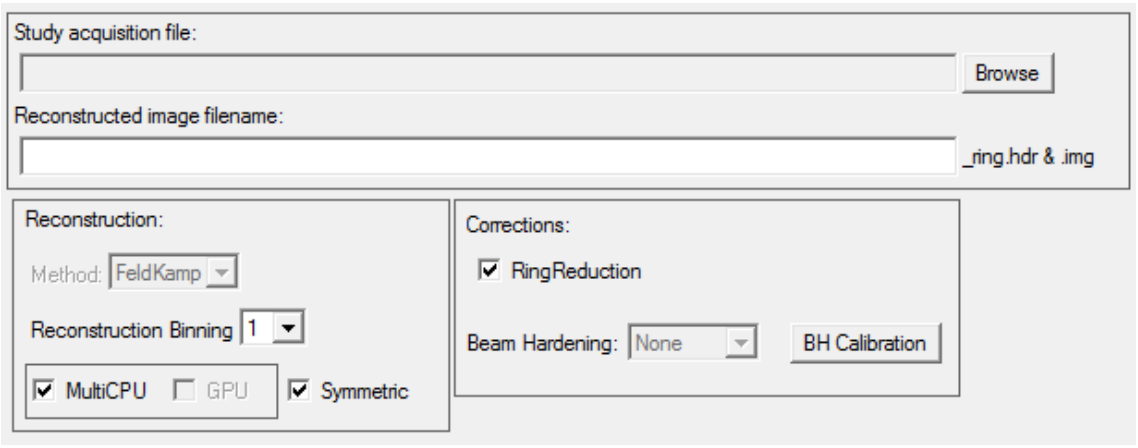

Figure 22. CT reconstruction interface in MMWKS

Ring Reduction correction was applied to CT images in order to attenuate ring artifacts (Figure 23). These concentric rings are caused by defective detector

elements, drifts in detector element sensitivity and non-linear responses to the incoming signal.

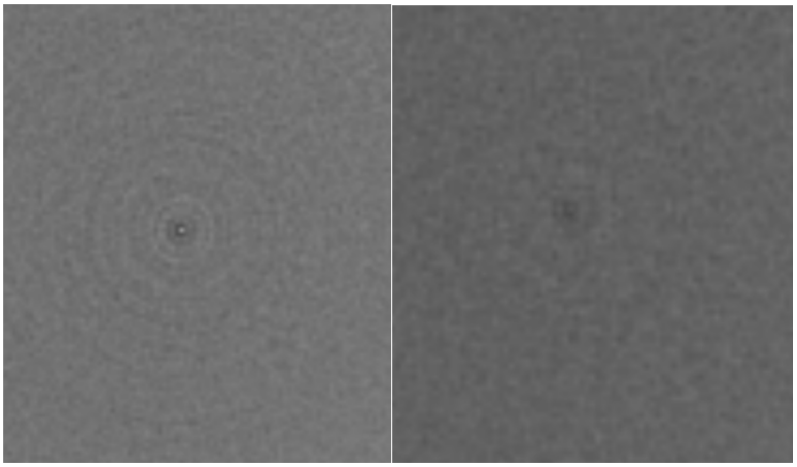

Figure 23. Ring artifact (CT image). Before Ring Reduction correction (left) and after applying the correction (right)

PET reconstruction

PET images were reconstructed with different algorithms: two iterative methods, (OSEM2D and OSEM3D) and an analytical method (FBP). The following default reconstruction parameters were set:

- FBP: Span 3, Dmax 16, ramp filter with alpha 1.0 and cutoff 1.0 (Figure 24).
- OSEM 2D: Span 3, Dmax 16, 2 iterations and 16 subsets (Figure 25).
- OSEM 3D: 2 iterations and 50 subsets (Figure 26).

Two iterations were selected because it is the most used number of iterations in rats and mice studies. The corrections applied to PET images were *Random* correction, *Scatter* correction and *Attenuation* correction. In this document, the term "non-attenuation corrected (NAC)" images refers to PET images corrected only by random and scatter, and the term "attenuation corrected (AC)" images (AC) refers to ones corrected by random, scatter and attenuation.

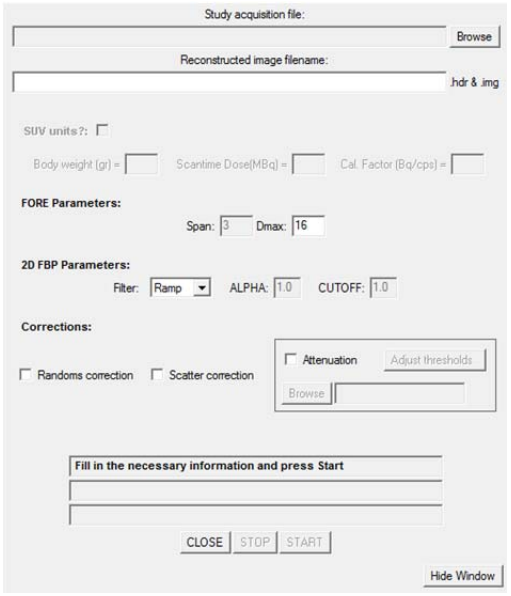

Figure 24. PET FBP reconstruction interface in MMWKS

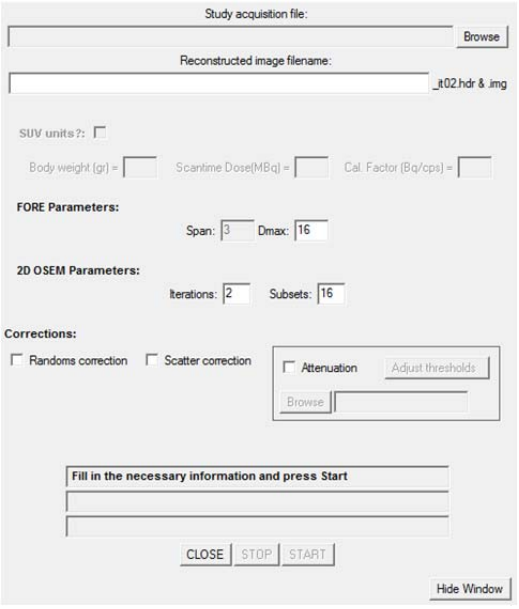

Figure 25. PET OSEM 2D reconstruction interface in MMWKS

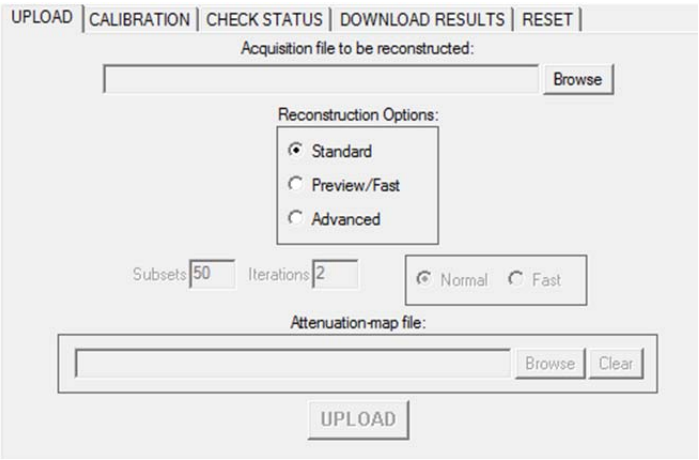

Figure 26. PET OSEM 3D reconstruction interface

3.1.4 Image segmentation

PET data used for the evaluation of the attenuation correction was obtained from a mask drawn on the radioactive point source of the corresponding CT image and then superimposed on the corresponding PET image. VOIs were not directly segmented on PET images because of PET blurred edges. An optimal PET mask is the one that covers at least 2 times the PET spatial resolution in each direction. In this study, a cylindrical mask of 2 mm diameter and 3.5 mm height was manually drawn on every CT image by using MMWKS (Figure 27). Before segmenting the images, it is necessary that both PET and CT images were registered. Although PET/CT studies acquired with the Argus PET/CT scanner are intrinsically registered, the slight misalignments were corrected by using the manual registration tool of MMWKS (Figure 28). The registration was checked by visual inspection with the fusion tool of MMWKS (Figure 29).

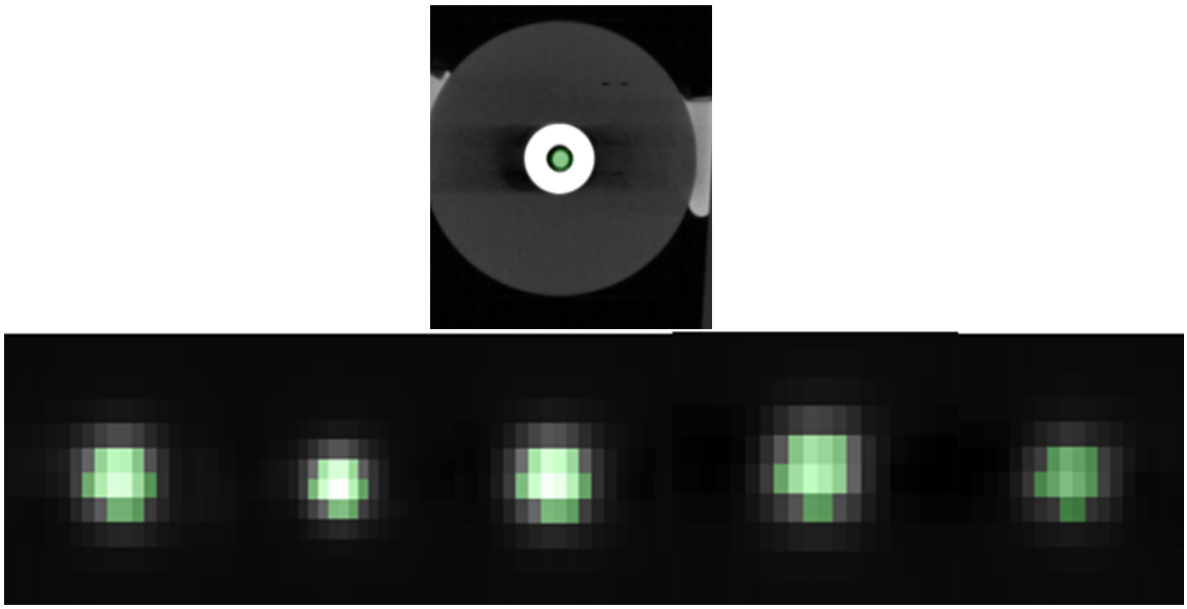

Figure 27. Segmentation mask (Study I). Mask (green) superimposed on CT image (coronal view, top) and several coronal slices of the mask superimposed on PET image (bottom)

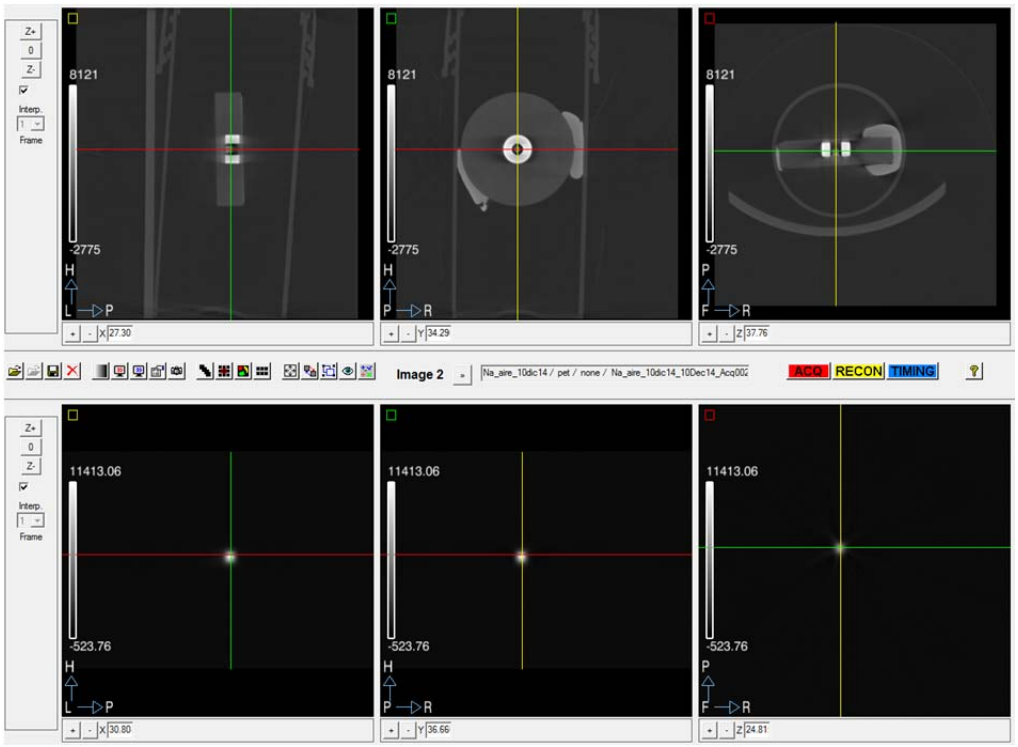

Figure 28. Registration interface in MMWKS

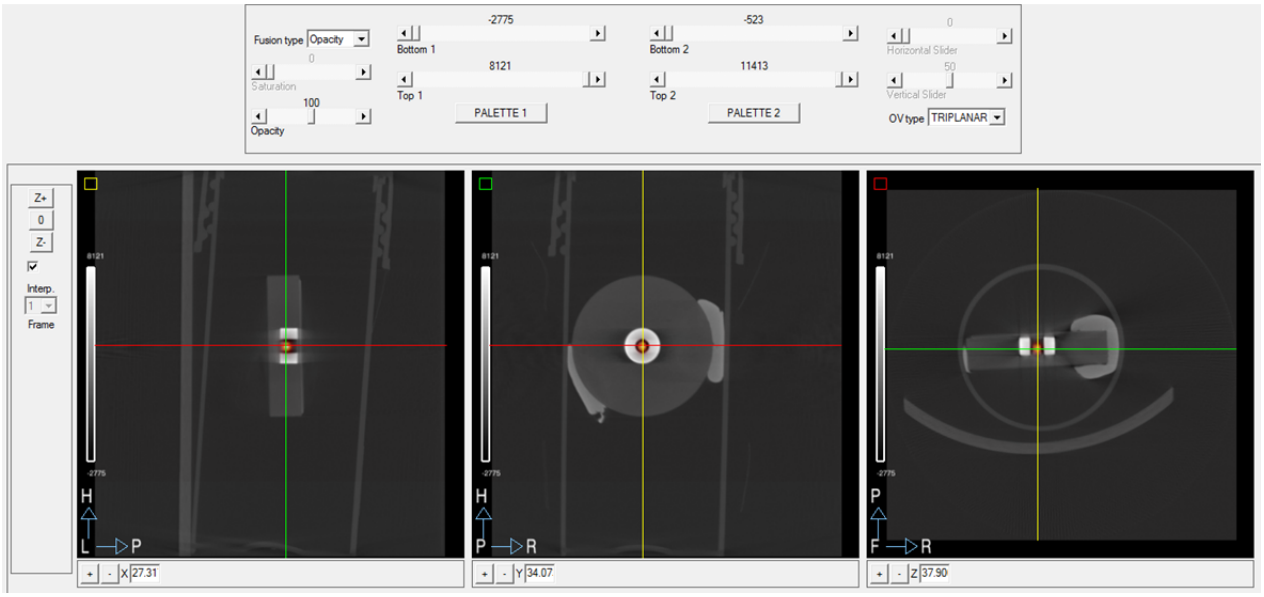

Figure 29. Fusion tool in MMWKS

3.1.5 Evaluation

The percentage of change was calculated in order to quantify the effect of applying the attenuation correction on PET images. This parameter measures the relative difference between the data extracted from the corrected image and the one from the non-corrected image. That data used was the mean value of the PET VOI given in cps and was obtained with MMWKS (Figure 30).

$$\%\ \boldsymbol{of\ change} = \frac{\boldsymbol{mean\ value\ of\ corrected\ image\ -\ mean\ value\ of\ non{-}corrected\ image}}{\boldsymbol{mean\ value\ of\ corrected\ image}}\ \boldsymbol{x\ 100}$$

Three percentages of change were calculated for the phantom with air medium and other three for the phantom filled with water.

To quantify the accuracy of the attenuation correction, the relative error between the mean VOI values of attenuation corrected images in air and water media was computed.

$$\text{Error}\ (\%) = \frac{mean\ value\ of\ water\ media\ AC\ image - mean\ value\ of\ air\ media\ AC\ image}{mean\ value\ of\ air\ media\ AC\ image}\ x\ 100$$

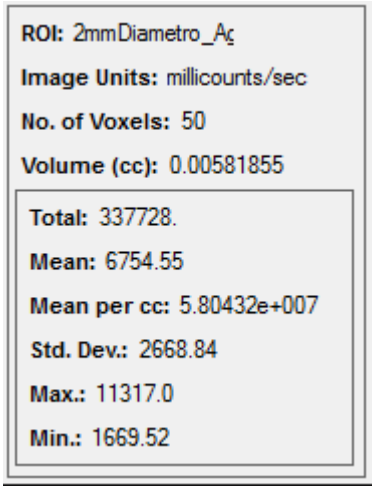

Figure 30. Statistics of the PET VOI

3.2 STUDY II: Activity concentration accuracy

The aim of this study was to evaluate the effect of the attenuation correction on the activity concentration accuracy. This study was performed using different energy windows and different reconstruction methods.

3.2.1 Phantom characteristics

NEMA-NU4 2008 image quality phantom was used in this study (Figure 31 and Figure 32) [14]. It is made of polymethylmethacrylate and has three main parts: a first part that has five rods of different diameters (1 mm, 2 mm, 3mm, 4 mm and 5mm) and 20 mm height that are filled with a radioactive solution and are used to calculate the recovery coefficients; a second part (30 mm diameter and 15 mm height) that is filled with a radioactive solution and is the region for uniformity measurements; and a third part that has two cold region chambers (one for air and other for nonradioactive water) surrounding by a radioactive solution and is used to obtain spill-over ratios.

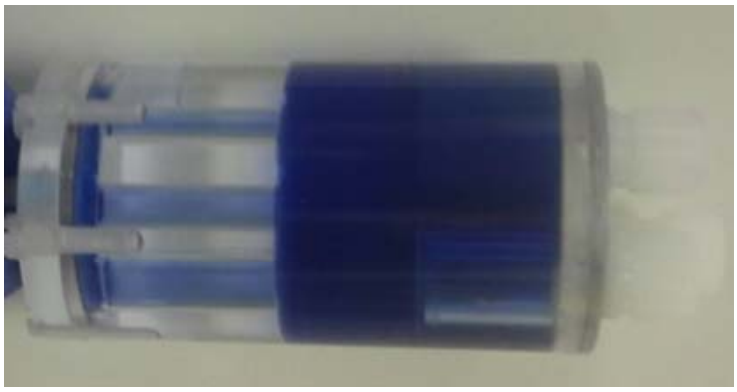

Figure 31. NEMA- NU4 2008 image quality phantom

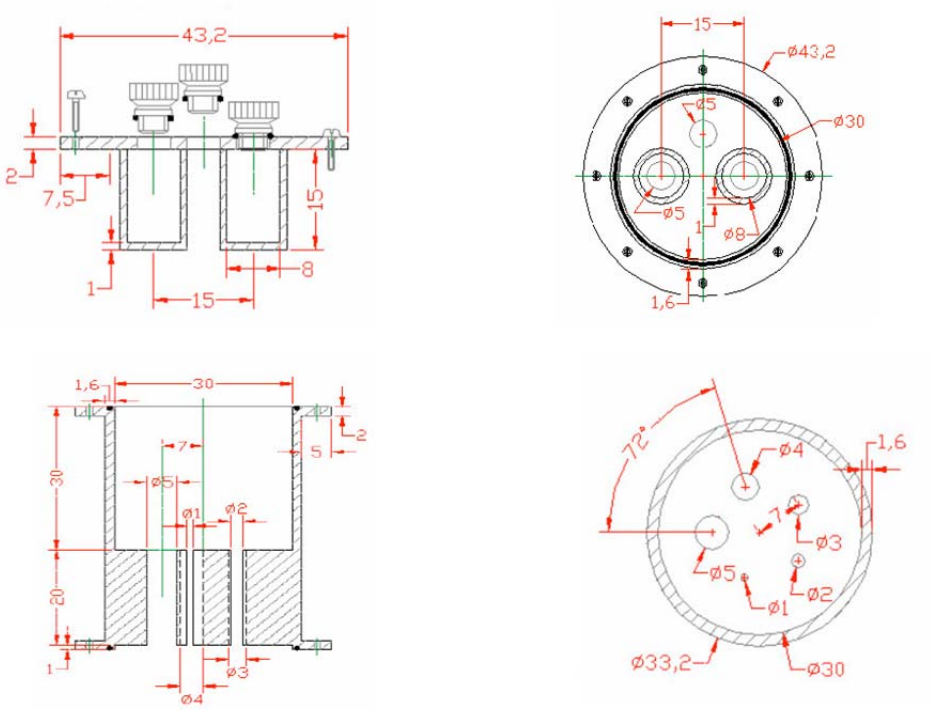

Figure 32. NEMA-NU4 2008 phantom design. Coronal (left) and transverse (right) cross sections [14]

The phantom was filled with a homogeneous dilution of the radiopharmaceutical FDG and water. NEMA protocol suggests that the activity used in the whole phantom shall be 100 µCi within ± 5% as calibrated at the start of imaging. This activity shall be within the range of the total activity used in mouse studies. The glucose support molecule does not alter the radioactivity characteristics of the radioisotope. Therefore, the complex has the same radioactivity characteristics as free F-18 (Table 4). All bubbles of the dilution were removed.

Isotope	**F-18**
Half- life [min]	**109.77**
Initial activity inside phantom (7Nov.2014, 15:50:46) [µCi]	**≈ 127.38**

Table 4. F-18 radioisotope characteristics (Study II)

3.2.2 Image acquisition protocol

One CT image and three PET images were acquired using the same settings as in Study I. Each PET image was obtained with a different energy window. The same CT image was used to generate the attenuation map that was applied to the three PET images. Figure 33 shows the scout and the PET volume acquired.

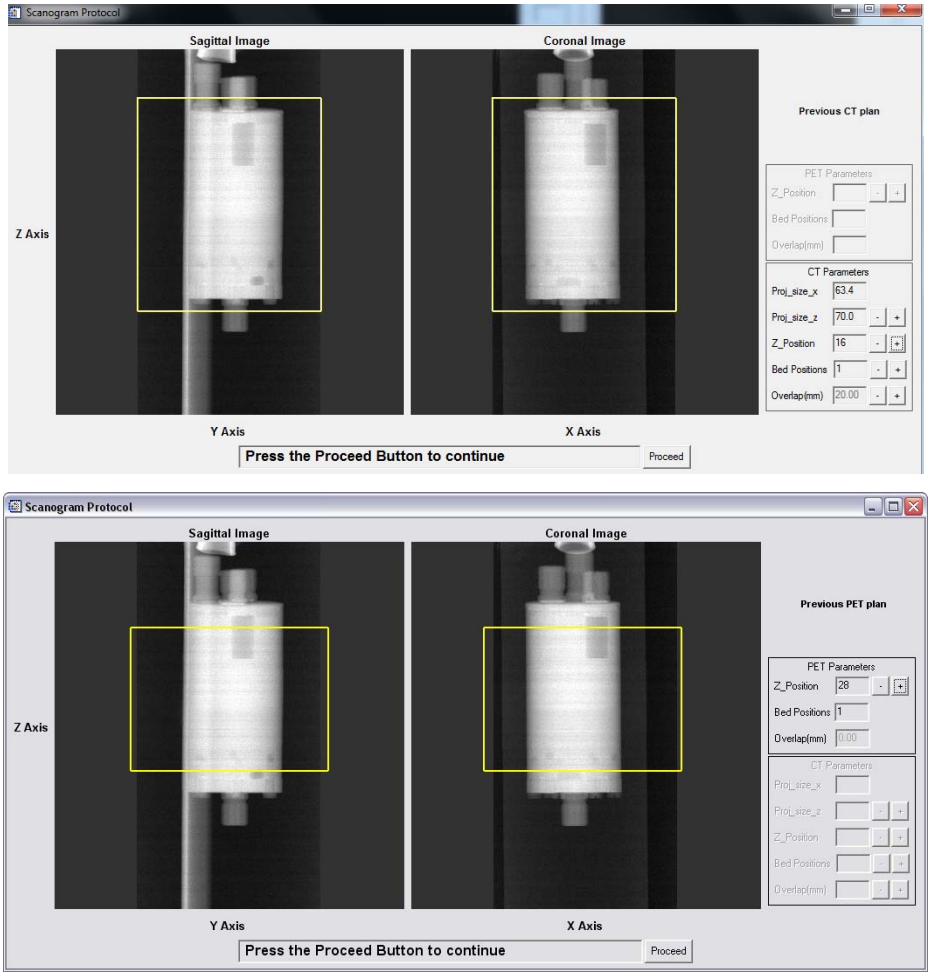

Figure 33. PET/CT acquisition (Study II). Scout images of NEMA- NU4 2008 phantom (top) and PET acquisition FOV (bottom). Yellow rectangles show the PET/CT acquisition FOV

3.2.3 Image reconstruction

The PET/CT study was reconstructed and corrected following the same protocol as in Study I with the exception of the number of iterations in OSEM 2D and OSEM 3D algorithms. In this case, PET images were reconstructed with one iteration in order to avoid over-iteration.

3.2.4 Image segmentation

In this study, the homogeneous part of the NEMA phantom was segmented on the PET images by using MMWKS. Following NEMA protocol, a cylindrical mask of 22.5 mm diameter and 10 mm height was drawn in order to obtain a uniformity measurement (Figure 34). The mask was not delineated on the CT image because the VOI was placed centred and inside the homogeneous part, and far from the phantom edges.

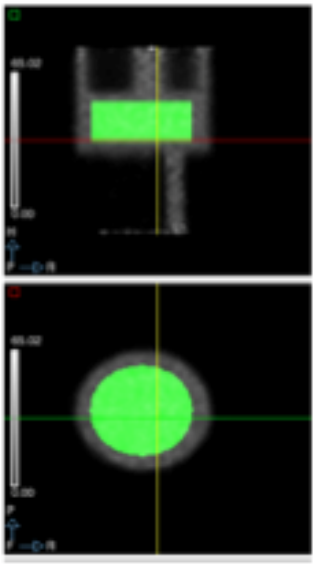

Figure 34. Segmentation mask (Study II). Mask (green) superimposed on PET image. Coronal view (top) and axial view (bottom)

3.2.5 Evaluation

The evaluation of the effect of the attenuation correction on the concentration accuracy was made by comparing the activity concentration given by the PET image with the real activity concentration value. The percentage of the relative error between both concentrations was calculated using the following equation:

$$Error\ (\%) = \frac{real\ activity\ concentration - image\ activity\ concentration}{real\ activity\ concentration}\ x\ 100$$

Real activity concentration

The real activity inside the phantom was directly measured by a well counter. To get reliable data the measurement was done at least three times and the real activity at the beginning of the experiment was the average of those measurements. The activity was 127.4 uCi.

To know the activity at the beginning of each PET acquisition (one per energy window, Table 5), the radioisotope decay has to be taken into account. The real activity concentration for each PET image was obtained by dividing the real activity at the beginning of each PET acquisition by the total volume introduced in the phantom (19.71 cc). Then, activity concentration was transformed from µCi/cc into Bq/cc.

Energy window	**Real activity at acquisition time [uCi]**
250-700 keV (16:17:13)	≈ 107.77
400-700 keV (16:40:46)	≈ 92.89
100-700 keV (17:03:15)	≈ 80.60

Table 5. Real activity for each PET acquisition (Study II)

Image activity concentration

The mean value of the PET VOI divided by the VOI volume in cc was extracted from the statistical report of MMWKS. This measurement was multiplied by the corresponding calibration factor in order to change cps/cc into Bq/cc. Several calibration factors were obtained depending on the reconstruction methods and on whether applying attenuation correction when obtaining this factor.

3.3 STUDY III: Effect of the attenuation correction on the recovery coefficient

The third experiment was focused on evaluating the effect of the attenuation correction on the recovery coefficient (RC). This parameter measures the change in activity concentration as a function of partial volume and gives information of the minimum object size to get reliable data.

This study was carried out by using the same images acquired in the Study II. Therefore, phantom characteristics, image acquisition protocol and image reconstruction were the same as in Study II.

3.3.1 Image segmentation

Two different segmentation protocols were compared: one following NEMA protocol and other one applying the usual idea in quantification of segmenting just the object size regarding the rods segmentation. In both cases the masks were directly drawn on PET images.

Following NEMA segmentation rule

NEMA protocol explains that the following masks should be drawn for the RC computation of each rod:

- Uniformity mask: Mask drawn in the homogeneous region of the phantom. It has to be a cylindrical mask of 22.5 mm diameter and 10 mm height (Figure 35).
- Rod mask: Draw a circular mask with a diameter twice the physical dimension of the rod on a 2D image that was generated by averaging the axial slices of the PET image covering the central 10 mm length of the rod (Figure 35).

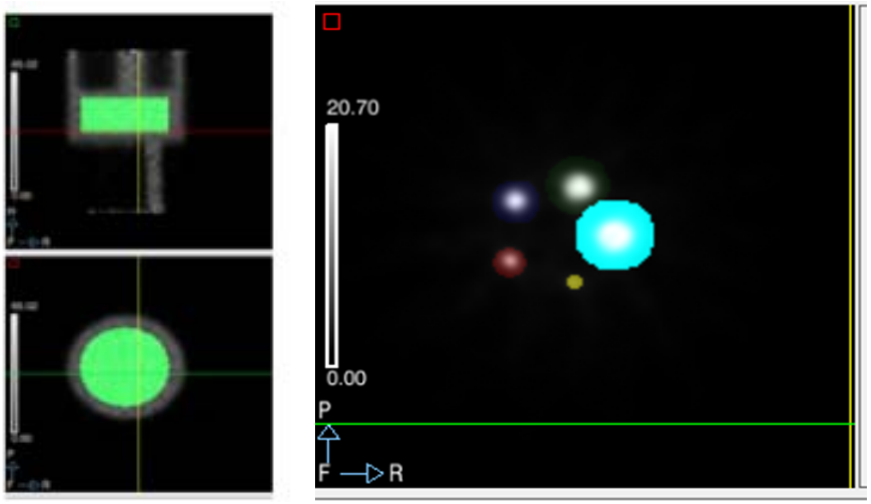

Figure 35. Masks drawn for RC computation following NEMA segmentation rule (Study III). Uniformity mask (green) superimposed on PET image (coronal view on the top left and axial view on the bottom left) and rod masks (several colours) superimposed on the average PET image (right)

Not following NEMA segmentation rule

In this case, the following masks were drawn:

- Uniformity mask: The same mask that was obtained following NEMA segmentation rule (Figure 35).

- Rod Mask: Draw a circular mask with a diameter equal to the physical dimension of the rod on the same 2D averaged image when following NEMA segmentation rule (Figure 36).

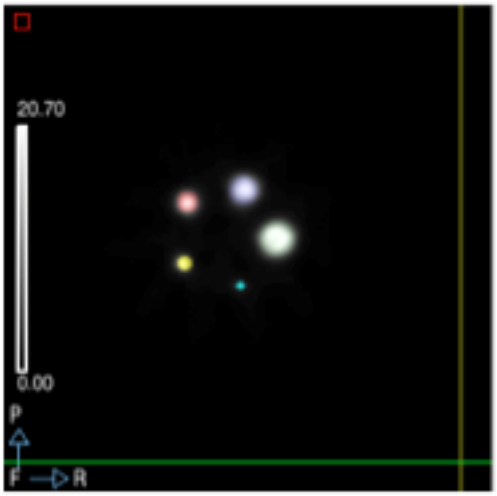

Figure 36. Rod masks when not fulfilling NEMA segmentation rule

3.3.2 Evaluation

The effect of the attenuation correction on the RC was evaluated taking into account different PET energy windows and different reconstruction methods on PET images without attenuation correction and after applying this correction. The RC and the standard deviation of the RC (STD_{RC}) were calculated following the NEMA protocol and using the masks previously mentioned. This procedure defines the RC value as the ratio between the mean value of a line profile and the mean value of the uniform region [14, 15]:

$$RC\ (\%) = \frac{mean\ value\ of\ the\ line\ profile}{mean\ value\ of\ the\ unifom\ region}\ x\ 100$$

The mean value of the uniform region is extracted directly from the MMWKS report by using the uniformity mask. The mean value of the line profile for each rod was computed as follows. First, find the maximum value of a particular rod in its mask either following NEMA segmentation rule or not. Then, localize the pixel coordinates of the maximum value. Finally, obtain the mean value of the line profile drawn in the PET image using the same axial slices that were previously averaged and localized at the pixel coordinates of the maximum value.

RC measures the difference between the measured activity concentration of a small object (measurement with partial volume effect) and the measured activity concentration of a large object that was filled with the same activity concentration [14, 16-18]. If both activity concentrations are equal, RC (%) is 100. When analysing PET studies is very common to use the mean value of a VOI instead of the mean of several maximum values as was done with RC. In this study, another recovery coefficient (RC2) was calculated using the mean value of the VOI instead of the mean value of the line profile in order to test how different is the activity concentration in each rod when compared to the uniformity activity concentration.

$$RC2(\%) = \frac{mean\ value\ of\ the\ VOI}{mean\ value\ of\ the\ uniform\ region}\ x\ 100$$

The STD_{RC} of each rod was calculated using the following equation [14, 15]:

$$\%\ STD_{RC} = 100\ x\ \sqrt{\left(\frac{STD_{\ line\ profile}}{Mean_{\ line\ profile}}\right)^2 + \left(\frac{STD_{\ uniform\ region}}{Mean_{\ uniform\ region}}\right)^2}$$

where $STD_{\ line\ profile}$ is the standard deviation of the values of the line profile previously mentioned, $Mean_{\ line\ profile}$ is the mean of the values of the line profile, $STD_{\ uniform\ region}$ is the standard deviation of the uniform region (hot background) and $Mean_{\ uniform\ region}$ is the mean of the uniform region.

4. RESULTS and DISCUSION

This section describes the results of three experiments performed in order to evaluate the CT-based attenuation correction on PET images acquired with the small animal Argus PET/CT scanner.

4.1 STUDY I: Accuracy of the attenuation correction on PET studies

This first study assessed the effect of applying the attenuation correction on PET images acquired with different energy windows and reconstructed with different methods. Figure 37, Figure 38 and Figure 39 show the activity of the VOI drawn on the radioactive point source of the air phantom depending on the reconstruction method and for each energy window respectively. Table 6 describes the percentage of change when applying the attenuation correction on images of this phantom. Figure 40, Figure 41, Figure 42 and Table 7 show those same types of results in the water phantom. Table 8 shows the relative error between attenuation corrected images in air and water media.

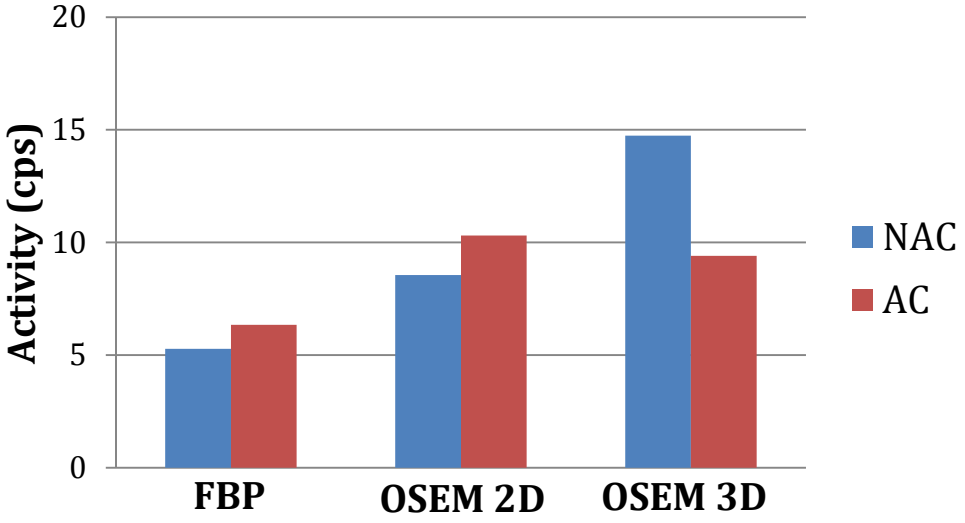

Figure 37. Air phantom VOI activity (100-700 keV)

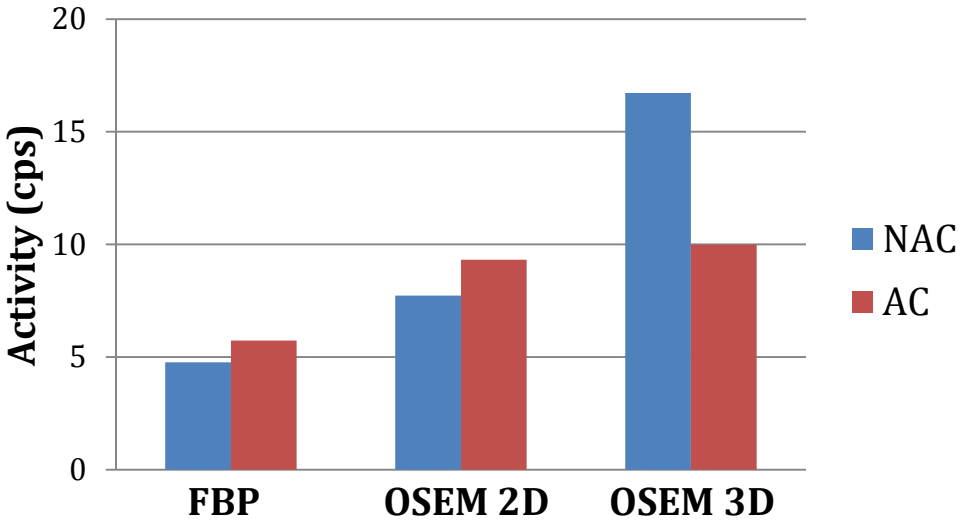

Figure 38. Air phantom VOI activity (250-700 keV)

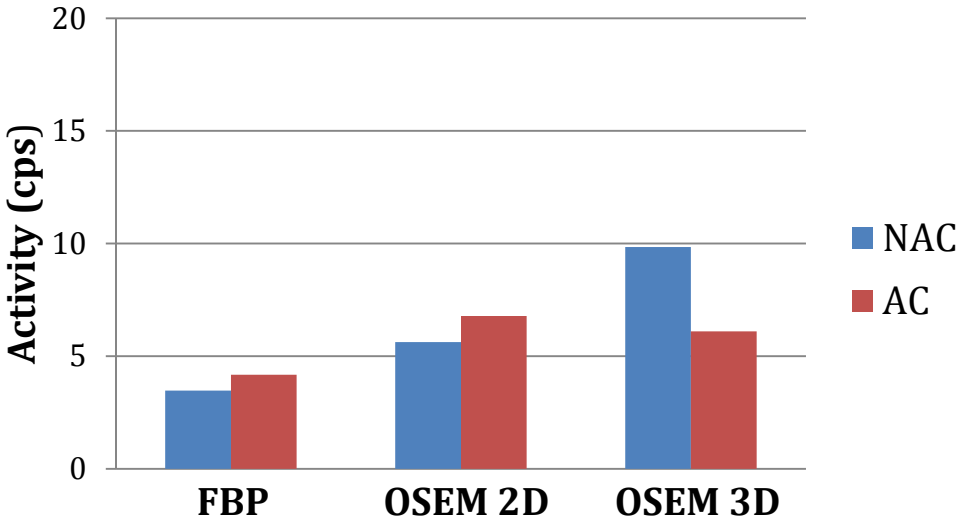

Figure 39. Air phantom VOI activity (400-700 keV)

% of change	100-700 keV	250-700 keV	400-700 keV
FBP	18.61	16.80	16.80
OSEM 2D	17.03	17.01	17.11
OSEM 3D	36.18	40.26	30.04

Table 6. Percentage of change with air phantom

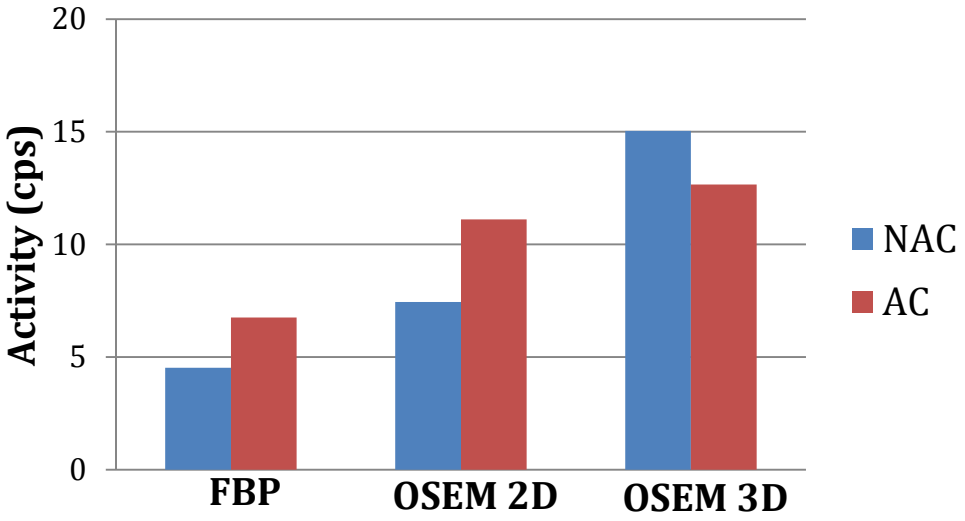

Figure 40. Water phantom VOI activity (100-700 keV)

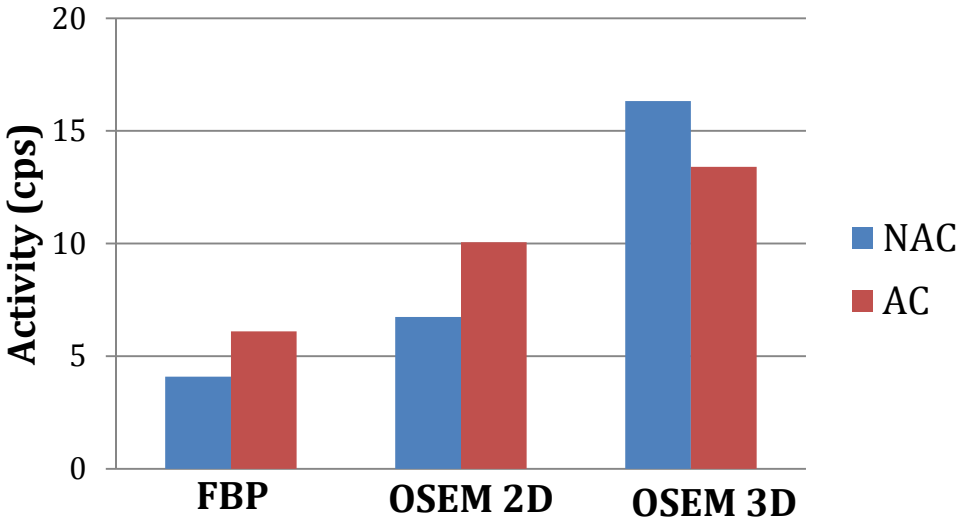

Figure 41. Water phantom VOI activity (250-700 keV)

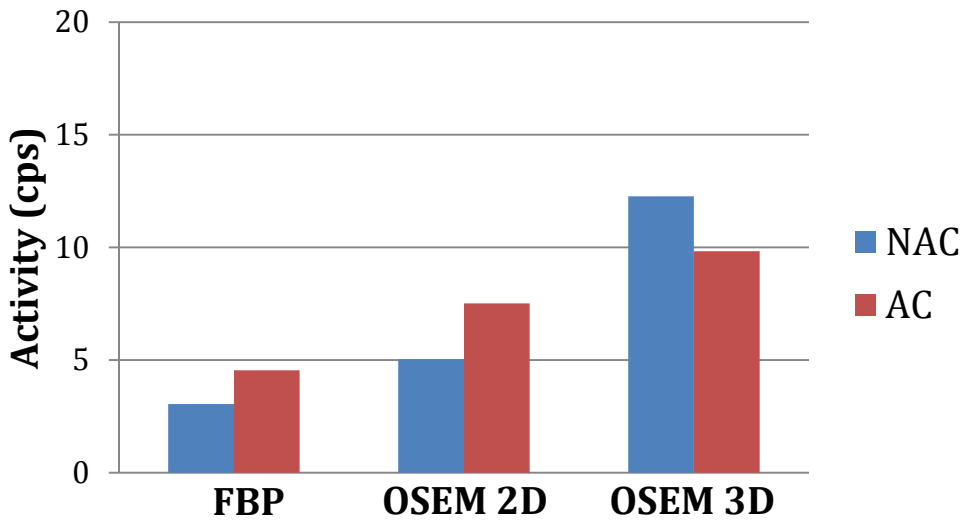

Figure 42. Water phantom VOI activity (400-700 keV)

% of change	100-700 keV	250-700 keV	400-700 keV
FBP	33.01	33.01	33.00
OSEM 2D	33.02	33.02	33.00
OSEM 3D	15.85	17.90	19.87

Table 7. Percentage of change with water phantom

Relative error (%)	100-700 keV	250-700 keV	400-700 keV
FBP	6.45	6.47	8.98
OSEM 2D	7.85	7.99	10.77
OSEM 3D	34.50	34.21	61.07

Table 8. Relative error between attenuation corrected images in air and water media

Regarding the above figures, the first overall result that can be observed is that the image activity (cps) in the radioactive point source VOI increases when applying the attenuation correction independently of the attenuation medium, the energy window and the reconstruction method except for OSEM 3D (activity decreases). This inconsistency is due to a different normalization criterion in the reconstruction algorithm. For OSEM 3D algorithm, the number of counts in

attenuation corrected images are adjusted to the total counts in the sinogram while for FBP and OSEM 2D that adjustment is performed in non-corrected images. FBP and OSEM-2D algorithms add an estimation of the attenuated counts to get the attenuation corrected images.

On the other hand, image activity of the radioactive source in the water medium is lower than in the air medium for non-corrected images with different energy windows and reconstruction methods (FBP and OSEM 2D). The reason is that water medium attenuates more photons than air medium. However, after applying attenuation correction, activity in water medium does not match exactly the one in air medium. The relative errors are lower than 9% for FBP, 11% for OSEM 2D but much higher for OSEM 3D.

Another result that can be observed is that the image activity (cps) in the radioactive point source VOI decreases with a narrower energy window independently of the attenuation medium and the reconstruction method, except for OSEM 3D, and of whether applying attenuation correction. A possible explanation for this decrease is that as the energy window is narrower less photons are able to be counted by the detector. On the other hand, the activity is higher in OSEM 2D than FBP independently of the other factors.

Regarding the percentage of change, values are almost similar in the case of FBP and OSEM 2D independently of the energy window, being higher for water medium (around 33%) than for air medium (around 17%). The reason of having changes around 17% in the phantom with air medium (air does not attenuate) may be due to the photon attenuation of the radioisotope encapsulation (first layer close to the radioisotope ≈ 6000 HU and second layer ≈ 200 HU) and less to the radioisotope walls of the universal sample tube (≈ 0 HU). Water medium results for FBP and OSEM 2D reconstruction methods are in accordance with [9]. This study showed a 31% of difference for a mouse phantom (using a syringe of 30 mm diameter) with an eXplore Vista scanner (General Electric) and linear attenuation coefficients at 511 keV for their implementation of CT-based attenuation correction. Moreover, in [11] the authors obtained a percentage of change for PET

transmission based attenuation correction around 3% while for CT-based attenuation correction the percentage of change was around 35% (microPET R4 system, Concorde Microsystems/Siemens, OSEM 2D reconstruction) based on their results of uniformity values (mean in nCi/cc). Mouse studies found in the literature describes percentages of change around 10% to 20% (MicroPET Focus 120 scanner, Concorde Microsystems/Siemens) [19] and 26% (eXplore Vista scanner, General Electric) [9], closer to our results. In the case of OSEM 3D, the percentage of change follows a different pattern than in OSEM 2D and FBP: values are higher in air medium than water medium.

4.2 STUDY II: Activity concentration accuracy

This second study assessed whether activity concentration after attenuation correction is reliable or not by using NEMA phantom.

Table 9 shows the calibration factor used to convert image activity from cps into Bq. This parameter varies depending on acquisition and reconstruction protocols. Therefore, a different calibration factor was applied to each PET image depending on the energy window, on the reconstruction method and whether attenuation correction was included. As attenuation correction can be also selected when obtaining this calibration factor, the NAC calibration factor was applied to NEMA phantom NAC PET images and AC calibration factor to NEMA phantom AC images.

Calibration factor (Bq/cps)	**100-700 keV**	**250-700 keV**	**400-700 keV**
FBP (NAC)	744.5	913.2	1453.7
FBP (AC)	512.1	627.8	1001.3
OSEM 2D (NAC)	685.9	842.1	1339.8
OSEM 2D (AC)	472.3	579.5	923.8
OSEM 3D (NAC)	629.7	587.2	902.9
OSEM 3D (AC)	779.0	740.3	1159.2

Table 9. Calibration factors

Table 10 shows the relative error between the real activity concentration and the image activity concentration.

Error (%)	100-700 keV	250-700 keV	400-700 keV
FBP (NAC)	3.98	3.28	2.89
FBP (AC)	-2.19	-2.80	-3.25
OSEM 2D (NAC)	3.48	2.74	2.50
OSEM 2D (AC)	-2.73	-3.39	-3.32
OSEM 3D (NAC)	3.24	1.99	2.71
OSEM 3D (AC)	-1.34	-3.18	-2.76

Table 10. Relative error between real and image activity concentrations

Independently of the energy window and the reconstruction method, the absolute relative error between the estimated and real activity concentration was smaller than 5%. This value is the maximum acceptable error and takes into account sources of error involved in the process of obtaining a PET image and the activity concentration measurements (well counter, weighing scale, calibration factor and VOI segmentation).

PET images with attenuation correction had negative relative error values while the non-corrected ones had positive relative error values. These result simply show that attenuation corrected images are over corrected while non-corrected images are under corrected. Relative errors of PET images with attenuation correction and without this correction were lower than 5% because NEMA phantom (uniformity region) is similar to the phantom used in the calibration protocol.

Figure 43 shows the image activity concentration for the energy window 250-700 keV depending on the reconstruction method and whether the attenuation correction was applied. Table 11 describes the percentage of change for this case.

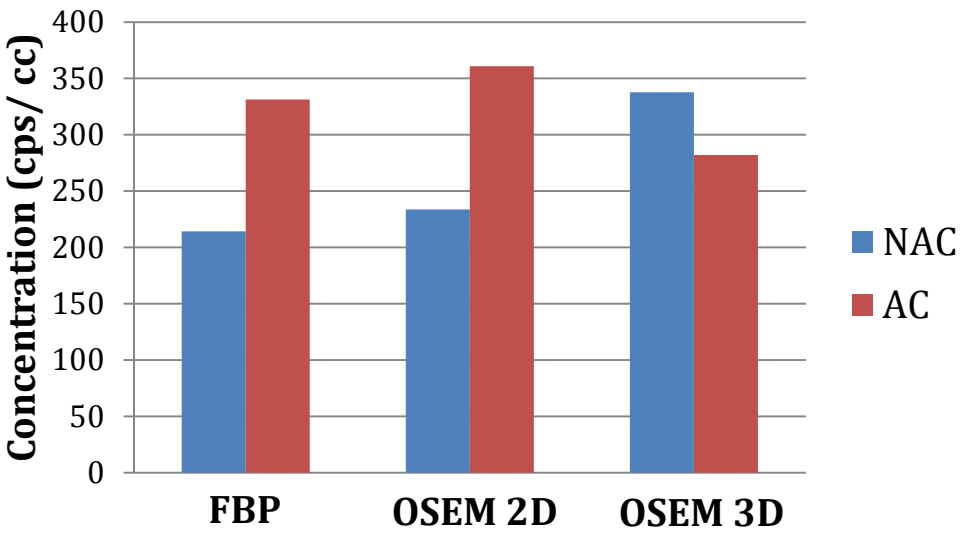

Figure 43. Comparative of image activity concentration at 250-700 keV

% of change	250-700 keV
FBP	35.33
OSEM 2D	35.26
OSEM 3D	19.75

Table 11. Percentage of change at 250-700 keV (Study II)

Similar conclusions can be extracted in this experiment as in the Study I: Image activity concentration increases in FBP and OSEM 2D methods when applying the attenuation correction while decreases in OSEM 3D due to algorithm normalization. The percentages of change show almost similar values than in Study I as both phantoms have almost similar dimensions and were filled with water. Slight differences could be due to the phantom used (NEMA phantom -diameter 43.2 mm- and not universal sample tube –diameter 30 mm- with radioisotope encapsulation) and radioisotope (F-18 and not Na-22). Conclusions extracted from 250-700 keV energy window are extrapolated to the other energy windows.

4.3 STUDY III: Effect of the attenuation correction on the recovery coefficient

This third and final study assessed the effect of the attenuation coefficient on RC with NEMA-NU4 2008 image quality phantom. This study was performed using different energy windows and reconstruction methods.

4.3.1 RC following NEMA segmentation rule

In this experiment, RC values were obtained following NEMA segmentation rule. Figure 44, Figure 45 and Figure 46 show the RC (%) for each rod and NAC/AC images depending on the energy window (100-700 keV, 250-700 keV and 400-700 keV respectively) for FBP reconstruction method. Table 12 summarizes the % STD_{RC} depending on those factors.

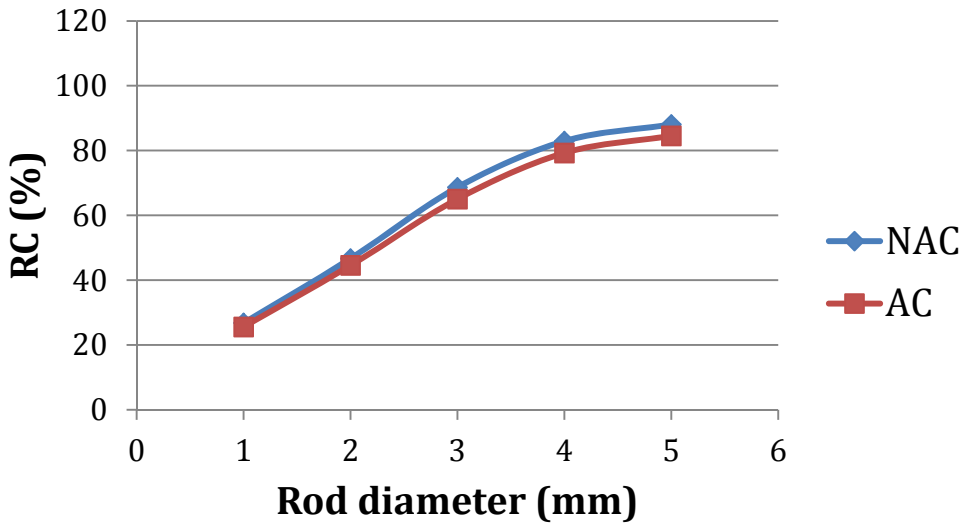

Figure 44. RC for FBP images acquired at 100-700keV

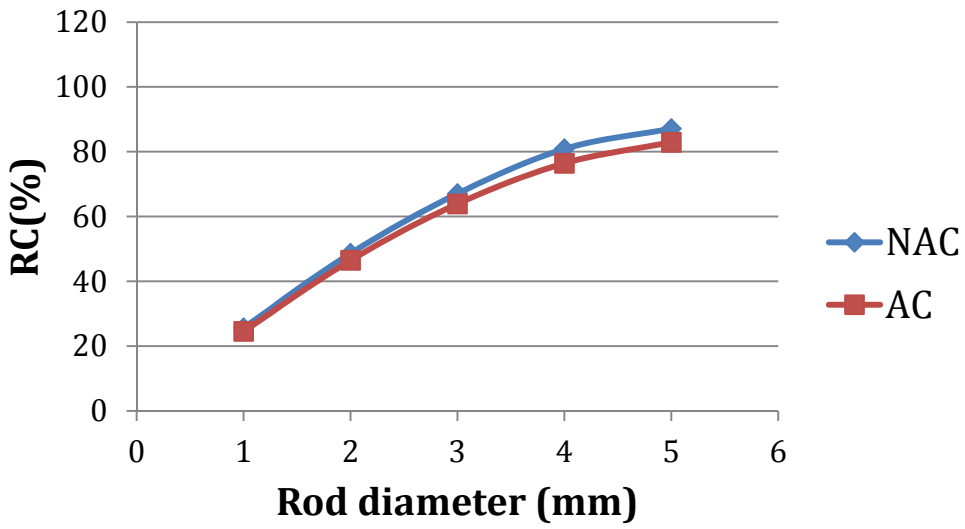

Figure 45. RC for FBP images acquired at 250-700 keV

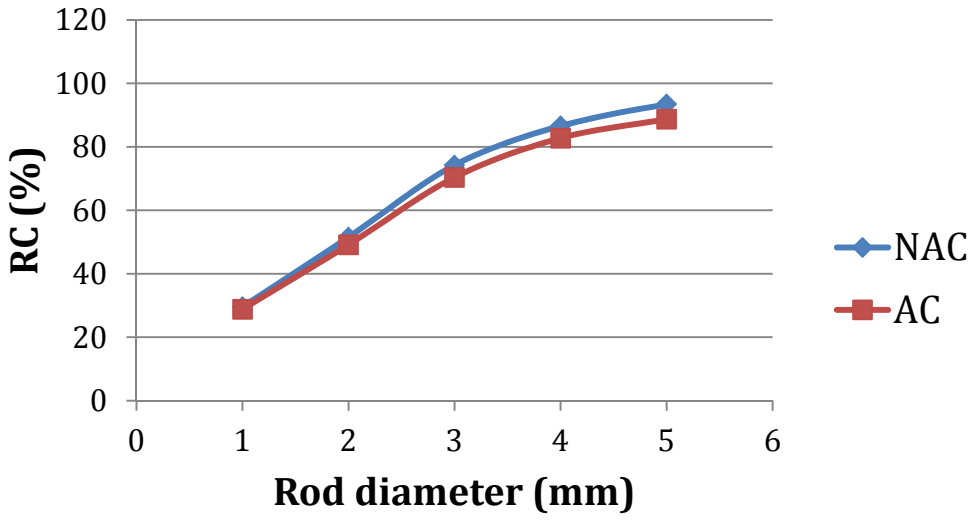

Figure 46. RC for FBP images acquired at 400-700 keV

% STD_{RC}	1mm	2mm	3mm	4mm	5mm
100-700 NAC	9.47	10.43	10.61	10.39	10.98
100-700 AC	9.94	10.23	10.47	10.08	10.69
250-700 NAC	8.45	9.18	6.95	8.89	5.70
250-700 AC	9.44	10.24	6.29	8.72	7.55
400-700 NAC	11.12	9.29	9.16	8.20	8.52
400-700 AC	10.43	5.02	8.70	7.60	8.90

Table 12. Standard deviation of RC for FBP reconstruction method

Figure 47, Figure 48 and Figure 49 show the RC (%) depending on the energy window (100-700 keV, 250-700 keV and 400-700 keV respectively) for OSEM-2D reconstruction method. Table 13 summarizes the % STD_{RC} for OSEM-2D.

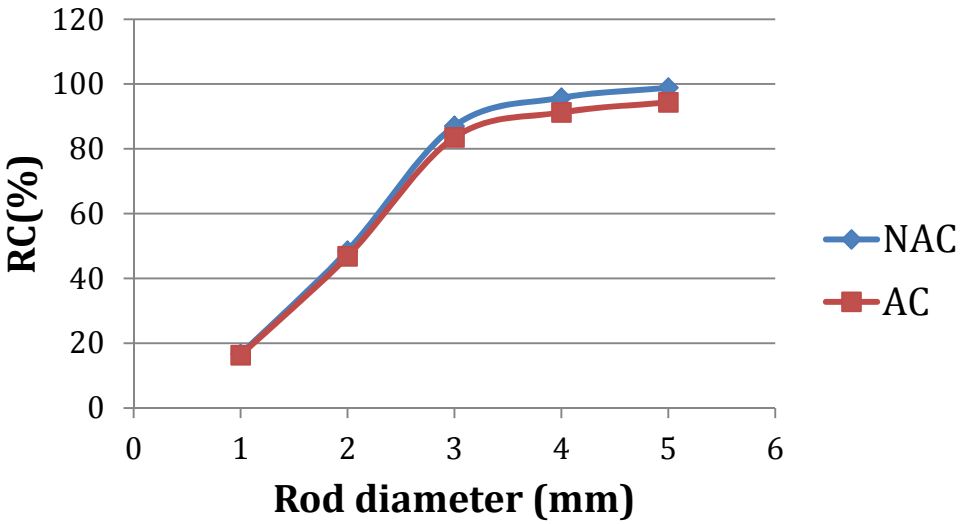

Figure 47. RC for OSEM 2D images acquired at 100-700 keV

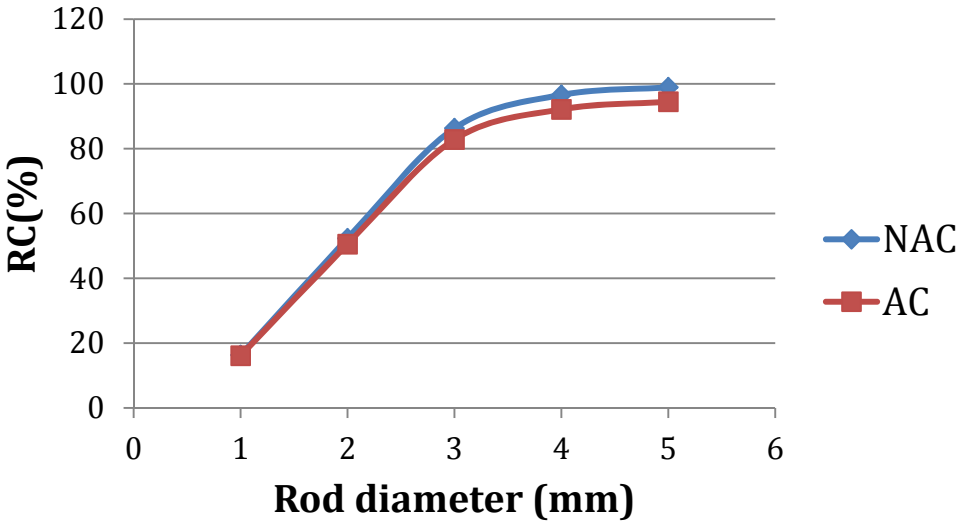

Figure 48. RC for OSEM 2D images acquired at 250-700 keV

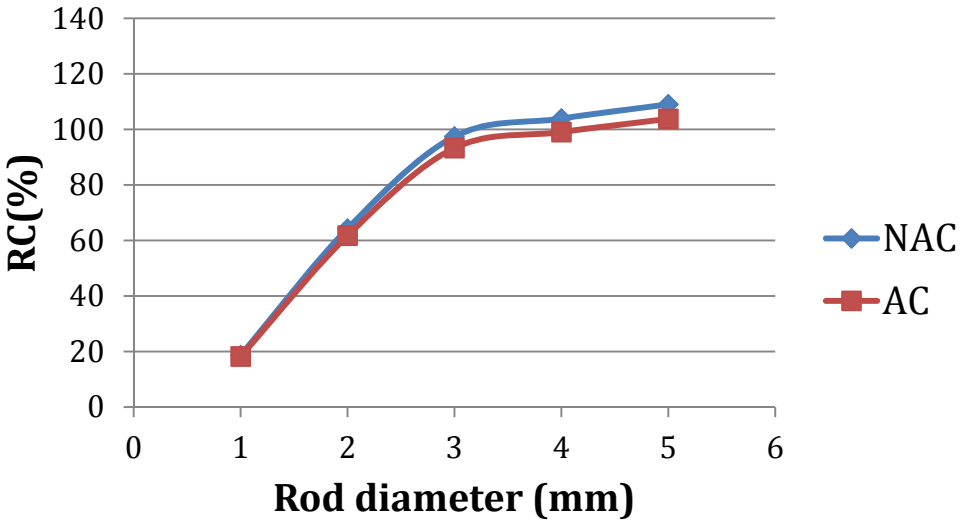

Figure 49. RC for OSEM 2D images acquired at 400-700keV

% STD_{RC}	1mm	2mm	3mm	4mm	5mm
PET 100-700 NAC	6.94	10.35	9.84	7.37	9.24
PET 100-700 AC	7.43	10.00	9.51	7.06	8.89
PET 250-700 NAC	9.49	10.26	8.28	7.65	6.55
PET 250-700 AC	7.80	8.66	7.90	7.31	6.15
PET 400-700 NAC	13.87	11.23	8.46	10.07	9.33
PET 400-700 AC	11.20	10.94	8.06	9.75	8.95

Table 13. Standard deviation of RC for OSEM 2D reconstruction method

Figure 50 shows RC values for OSEM 3D with 2 iterations (a usual reconstruction protocol in small animals). Depending on the energy window and whether applying attenuation correction, some RC values are higher than 100% that means that those PET images were over iterated. In order to overcome this over iteration, OSEM 3D images were reconstructed with one iteration and then filtered with a 3D Gaussian filter (standard deviation 0.5 mm).

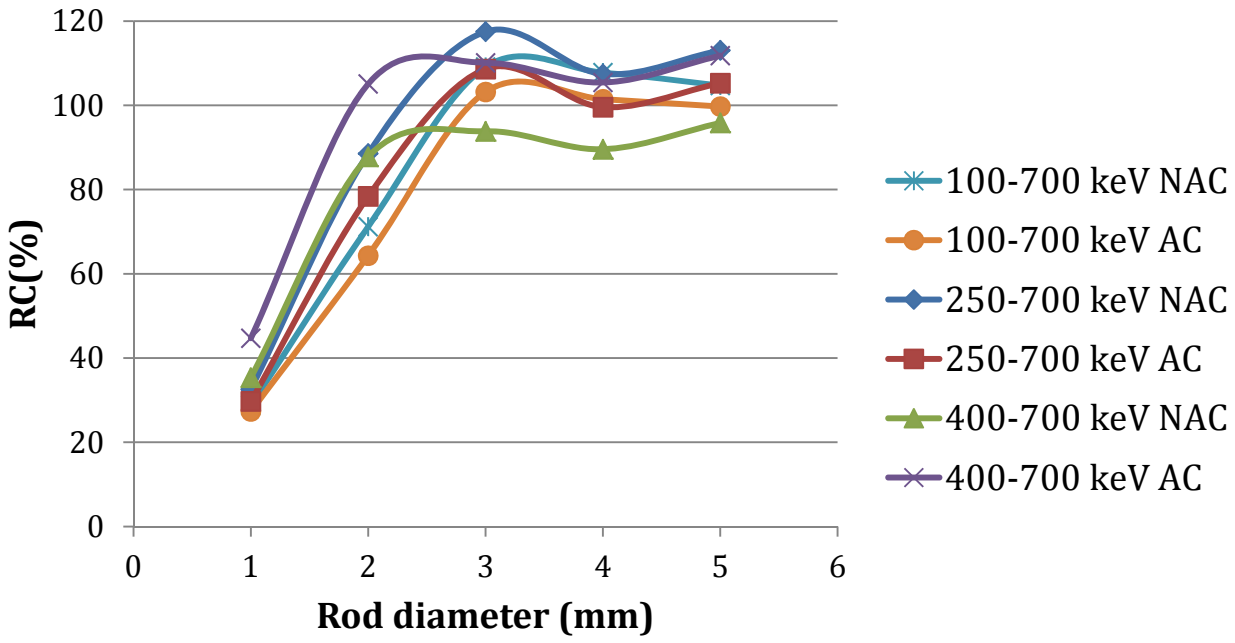

Figure 50. RC for over iterated OSEM 3D images

Figure 51, Figure 52 and Figure 53 show the RC (%) depending on the energy window (100-700 keV, 250-700 keV and 400-700 keV respectively) for OSEM-3D reconstruction method with one iteration and after filtering. Table 14 summarizes the % STD_{RC} for those OSEM-3D reconstructions.

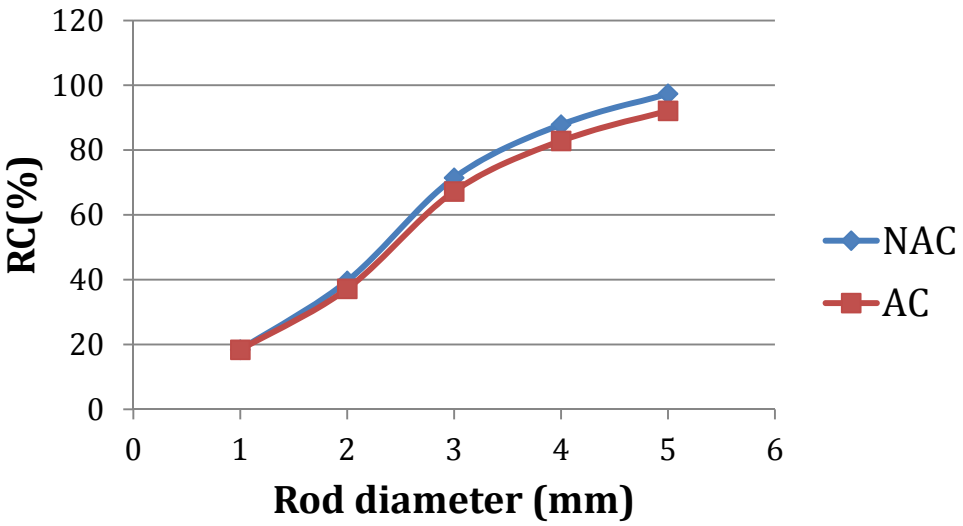

Figure 51. Filtered OSEM 3D RC for images acquired at 100-700 keV

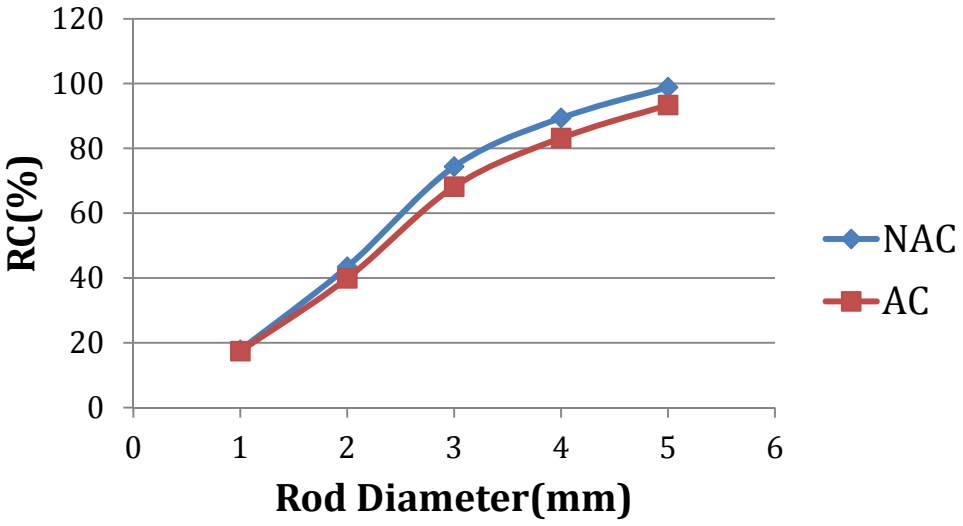

Figure 52. Filtered OSEM 3D RC for images acquired at 250-700 keV

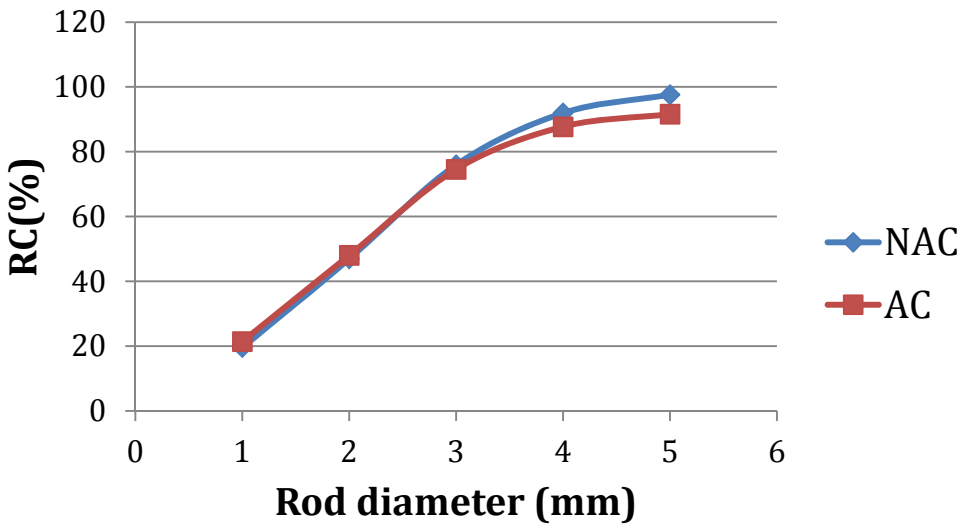

Figure 53. Filtered OSEM 3D RC for images acquired at 400-700 keV

% STD_{RC}	1mm	2mm	3mm	4mm	5mm
PET 100-700 NAC	4.68	5.50	5.69	4.38	4.13
PET 100-700 AC	6.46	4.19	4.86	4.06	4.31
PET 250-700 NAC	7.04	5.46	4.55	4.38	3.98
PET 250-700 AC	6.96	5.41	4.44	4.43	4.26
PET 400-700 NAC	6.09	5.95	5.33	5.36	4.88
PET 400-700 AC	6.48	6.15	5.12	5.34	5.29

Table 14. Standard deviation of RC for filtered OSEM 3D reconstruction method

Independently of the energy window, the reconstruction method and whether applying attenuation correction, the characteristic plot shape of RC is conserved. The activity concentration in the rods becomes more similar to the one of the homogeneous region as the rod diameter is larger. Moreover, the RCs of NAC images and AC images are similar except when rod diameter is close to 5mm. For that case, there are slightly differences.

Regarding the comparison of our results with the ones found in the literature, in [11] the authors showed the RC for non-attenuation corrected PET images and CT-based attenuation corrected PET images (microPET R4 system, Concorde

Microsystems/Siemens) scanner using an energy window of 350–650 keV and FBP, OSEM 2D and OSEM 3D reconstruction methods. Depending on the rod diameter, RCs for AC images are less than or equal to the ones of NAC images in accordance with our results. RC values are different from ours. For instance, RC values for rod of 3mm was 70%, 93% and 75% for FBP, OSEM 2D and OSEM 3D respectively in our case (400-700 keV, AC images) compare to 55%, 70% and 100% in their case. This could be because the scanner used is different. In [20], the authors compared several preclinical scanners such as microPET (P4, R4, Focus 120 and Focus 220; Concorde Microsystems/Siemens), Inveon (Siemens), Mosaic HP (Philips), ClearPET (Raytest GmbH), Argus (Sedecal), VrPET (Sedecal), LabPET (8 and 12; Gamma Medica). RCs from the Argus scanner were obtained with energy window of 250-700 keV, OSEM 3D, and scatter and attenuation corrections. Their results were 27%, 65%, 93%, 95% and 97% for rod diameter of 1 mm, 2 mm, 3 mm, 4 mm and 5 mm respectively and are higher than our results (17%, 40%, 68%, 83% and 93%). This could be due to the number of iterations used in OSEM3D and whether images were filtered. On the other hand, our RCs with energy window of 250-700 keV and FBP (24%, 47%, 64%, 76% and 83%, AC images) were slightly higher than those from microPET Focus 220 (15%, 41%, 63%, 74% and 86%, with scatter and attenuation corrections).

Regarding $\%STD_{RC}$, FBP images, OSEM 2D and OSEM 3D images have $\%STD_{RC}$ values lower than 12%, 14% and 8% respectively. In the literature, $\%STD_{RC}$ values were lower than 8% (FLEX Triumph PET/CT scanner, Gamma Medica, energy window 250-750 keV, FBP, OSEM 2D, CT-based attenuation correction) [21] , 10% (LabPET 8, energy window 250-650 keV, maximum-likelihood expectation maximization -ML-EM- reconstruction method, non-attenuation correction) [15], 12% (NanoPET/CT scanner, Bioscan Inc./Mediso Ltd., energy window 250-750 keV, ML-EM, non-attenuation correction) [22] or 15% (PETbox, ML-EM, CT-based attenuation correction) [23]. Our $\%STD_{RC}$ values are in accordance with the values previously presented.

Table 15, Table 16 and Table 17 summarizes the minimum object size in order to get reliable data depending on the reconstruction method for different energy

windows and AC images. That size was defined as the rod diameter needed to reach, at least, a RC of 90%. The minimum object size depends on the window energy and the reconstruction protocol (reconstruction method, number of iterations in the iterative algorithm), filtering...

Reconstruction Method	**FBP**	**OSEM 2D**	**OSEM 3D**
Diameter (RC %)	5 mm (90%)	3 mm (90%)	4 mm (90%)

Table 15. Minimum object size with a minimum RC of 90% (100-700 keV)

Reconstruction Method	**FBP**	**OSEM 2D**	**OSEM 3D**
Diameter (RC %)	5 mm (90%)	4 mm (100%)	4 mm (90%)

Table 16. Minimum object size with a minimum RC of 90% (250-700keV)

Reconstruction Method	**FBP**	**OSEM 2D**	**OSEM 3D**
Diameter (RC %)	5 mm (90%)	4 mm (100%)	5 mm (100%)

Table 17. Minimum object size with a minimum RC of 90% (400-700 keV)

4.3.2 RC not fulfilling NEMA segmentation rule

In this experiment, two segmentation methods were evaluated on obtaining RC values: one following NEMA segmentation rule and another one with a mask of diameter equal to the physical dimension of each rod.

Figure 54, Figure 55 and Figure 56 shows a comparison between segmenting following NEMA rule or not for OSEM 2D images (100-700 keV, 250-700 keV and 400-700 keV respectively). The mask size does not affect the RC value, independently of whether applying the attenuation correction. This is logical as far as the maximum value recorded using both methods is the same. This value is placed more or less in the middle of the rod and this region is always encircled by any of the masks used.

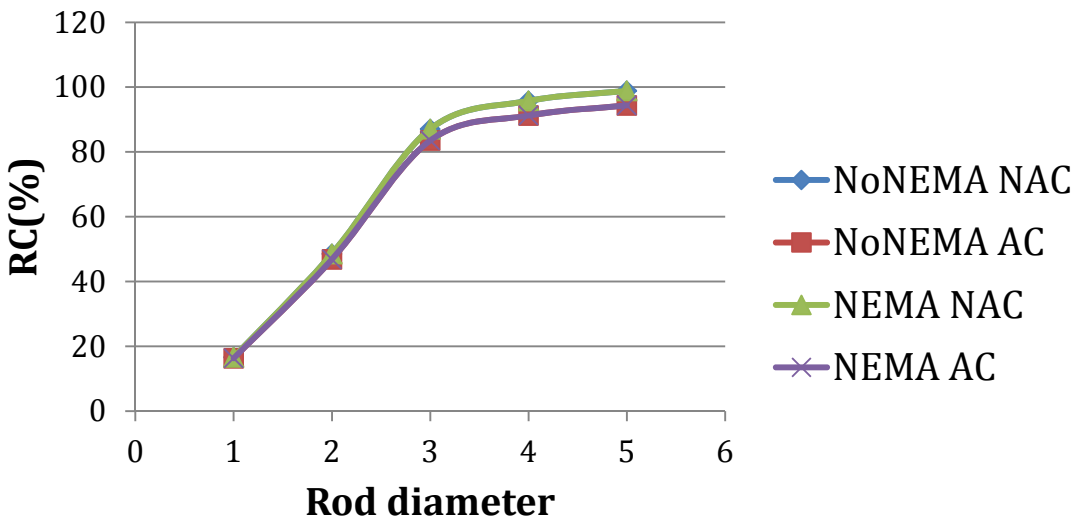

Figure 54. Comparison between both methods of segmentation in NAC/AC OSEM 2D images (100-700 keV)

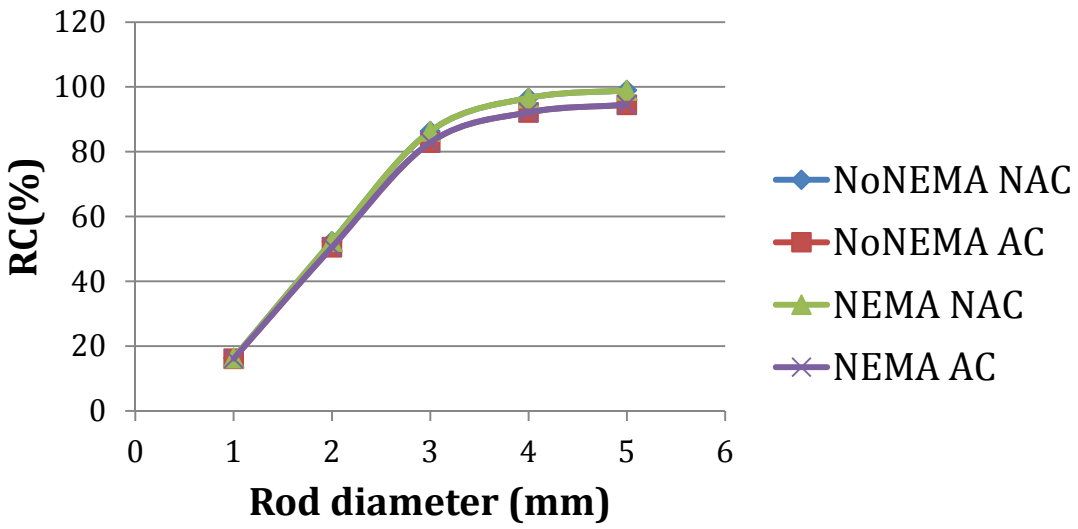

Figure 55. Comparison between both methods of segmentation in NAC/AC OSEM 2D images (250-700 keV)

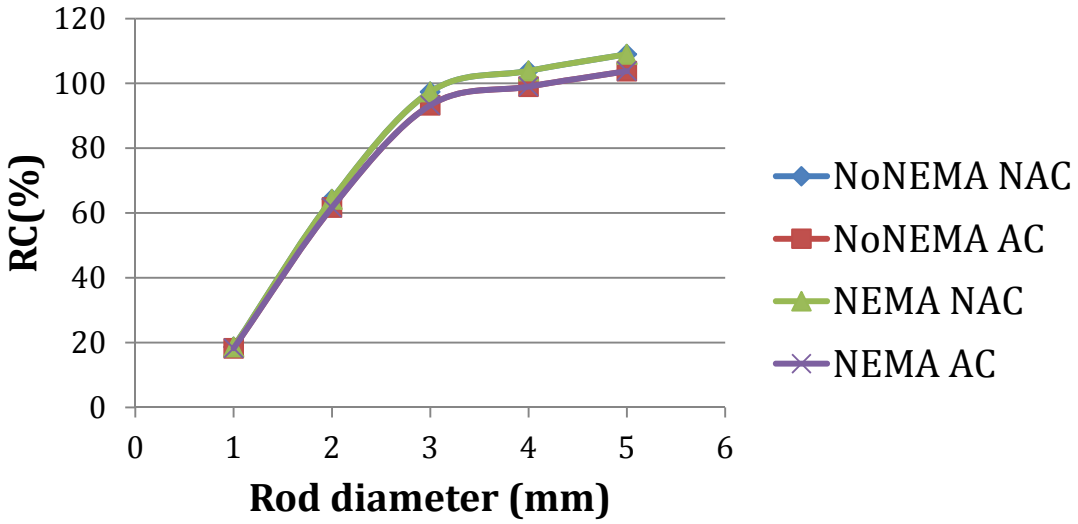

Figure 56. Comparison between both methods of segmentation in NAC/AC OSEM 2D images (400-700 keV)

4.3.2 Comparative of RC vs RC2

In this third experiment, two different RCs were calculated, one taking into account maximum values (NEMA definition, RC) and another one using the mean value of rod VOI (RC2). Both segmentation rules (following NEMA protocol or not) were also tested.

Figure 57 and Figure 58 show the comparison between RC and RC2 values following NEMA segmentation rule or not respectively. In both cases, NAC/AC images were acquired with the 400-700 energy window and reconstructed with OSEM 2D.

As in the previous experiment, the segmentation process does not affect RC. In the case of RC2, the segmentation process alters its values since increasing the mask size will include more background values and will decrease the VOI mean value. For instance, RC2 values following NEMA segmentation are close to 25% while not fulfilling NEMA gives RC2 values from 20% to 75%. Therefore, NEMA segmentation rule is not adequate for RC2 calculation.

Figure 58 plots are completely different. Although the shape is more or less the same, RC values are closer to 100% (rod diameter from 3 mm to 5 mm) than RC2 (75% for the largest rod). Therefore, when segmenting small objects, VOI mean value does not provide an accurate activity concentration. A better strategy in that case is to average maximum values of the VOI. Concerning attenuation correction, there are small differences in RC and RC2 values.

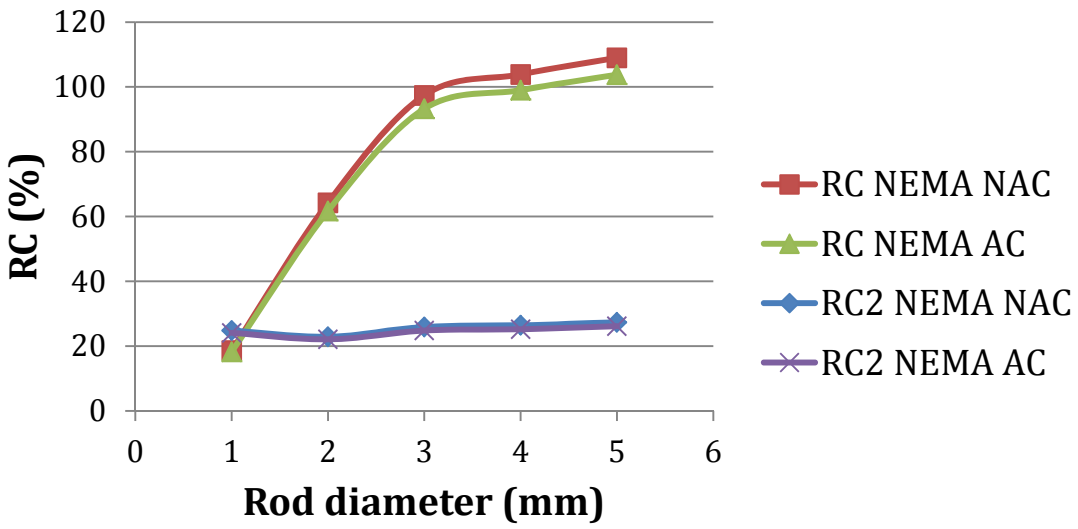

Figure 57. RC vs RC2 following NEMA segmentation rule

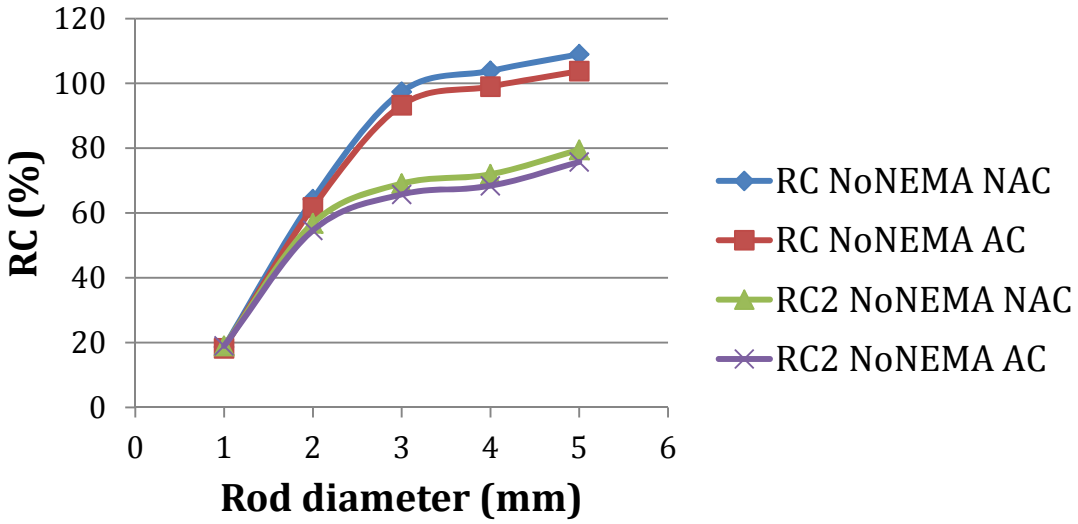

Figure 58. RC vs RC2 not fulfilling NEMA segmentation (No NEMA)

5. CONCLUSIONS AND FUTURE WORK

A comprehensive evaluation of the CT-based attenuation correction in an Argus PET/CT scanner was done in this bachelor thesis from a practical point of view (quantification results). Attenuation correction is important in order to obtain an accurate quantification of radiotracer activity concentration.

Attenuation correction has an impact on the image data and results are different depending on the Argus PET/CT reconstruction method used. For FBP and OSEM 2D reconstruction methods, image activity (cps) increases when applying the attenuation correction independently of the attenuation medium, the energy window but, for OSEM 3D, the activity decreases due to a different adjustment of the total counts in the sinogram. The percentage of change between non-attenuation corrected PET images and attenuation corrected PET images in the case of the water phantom (around 33%) is in accordance to the results obtained with a similar phantom in another study found in the literature. However, after applying attenuation correction, activity in water medium does not match exactly the one in air medium (worse results in the case of OSEM 3D reconstruction method).

The absolute relative error between the estimated and real activity concentration either for non-attenuation corrected PET images or attenuation corrected PET images was smaller than 5%. PET images with attenuation correction had negative relative error values (over corrected) while the non-corrected ones had positive relative error values (under corrected). The accuracy of activity concentration presented an acceptable value independently of attenuation correction image as calibration factor compensates the differences between those images (similar phantoms).

Recovery coefficients for non-attenuation corrected PET images are similar than the ones for attenuation corrected PET images. Recovery coefficients values depend on the energy window used. The segmentation rule does not affect the

recovery coefficient calculation. However, when segmenting small objects, VOI mean value does not provide an accurate activity concentration.

Future work includes evaluating the effect of the attenuation correction in the Argus PET/CT scanner on larger phantoms to simulate a rat instead a mouse. In that case, literature shows a percentage of change about 48% in a rat phantom (using a syringe of 50 mm diameter) [9]. Moreover, studies using phantoms that simulate a more realistic mouse or rat (regions with a different density to simulate air and bones and regions with different activity concentration) would be also recommended. Further analysis of activity concentration accuracy should be also performed.

6. BUDGET

This section describes an estimation of the cost of realization of project. The budget was divided into two groups:

- Personnel costs: Total remuneration payable to people working on the project.
- Material costs: Amount of money invested in software, hardware elements and fungible materials used in this project.

6.1 Personnel costs

Table 18 show the roles and costs associated with their work.

Category	Euros/hour	Total hours	Costs
Senior Consultant	50	20	1,000.00€
Consultant	36	100	3,600.00€
Laboratory technician	25	10	250.00€
Laboratory technician	25	10	250.00€
Junior engineer	20	350	7,000.00€
TOTAL	-	490	**12,100.00 €**

Table 18. Personnel costs

6.2 Material costs

The material was divided into software and hardware material. Table 19 describes the costs associated with the software used in this bachelor thesis. That software was MMWKS and Microsoft Office (Excel, Word, and PowerPoint). Regarding Office pack, the amount of money shown in this table refers to the cost of buying its license. Table 20 shows the costs related to hardware and fungible materials.

MATERIAL	Euros/hour	Total hours	Costs
MMWKS	25	240	6,000.00€
Office pack	-	-	119.00€
TOTAL	-	-	**6,119.00€**

Table 19. Software material costs

MATERIAL	Euros/hour	Total hours	Costs
Computer + office material	-	-	250.00€
PET/CT system + radiotracer	180	10	1,800.00€
Laboratory material	-	-	100.00€
TOTAL	-	-	**2,150.00€**

Table 20. Hardware and fungible material costs

6.3 Indirect costs

The indirect costs correspond to a 20% of the material and personnel costs, which corresponds to 4,073.80 € approximately.

6.4 General cost and industrial benefit

The general costs and industrial benefit correspond to 16% and 6% of the material costs respectively. Then the general costs are estimated to be 1,323.04€ and the industrial benefit 496.14€.

6.5 Total cost of the project

Table 21 describes the estimated total cost of this bachelor thesis. It amounts to **31,777.00** €.

TYPE of COST	Costs
Personnel costs	12,100.00 €
Software costs	6,119.00€
Hardware and fungible material costs	2,150.00€
Indirect cost	4,073.80 €
General cost	1,323.04€
Industrial benefit	496.14€
TOTAL (without taxes)	26,261.98 €
TOTAL (with taxes, 21%)	**31,777.00 €**

Table 21. Estimated total cost of the project

7. BIBLIOGRAPHY

1. Pascau J, et al. *Multimodality workstation for small animal image visualization and analysis.* Molecular Imaging and Biology, 2006. **8**(2): p. 97-98.
2. Molina C. *Corrección del artefacto de endurecimiento de haz (beam hardening) para imágenes obtenidas con tomógrafo de rayos X de pequeños animales.* Universidad Autónoma de Madrid, 2012.
3. Dilsizian V, Pohost GM. *Cardiac CT, PET and MR.* Wiley, 2011.
4. Bailey DL, et al. *Positron emission tomography: Basic sciences.* Springer London, 2006.
5. Shaw CC. *Cone Beam Computed Tomography.* Taylor & Francis, 2014.
6. López J. *Técnicas avanzadas de reconstrucción de imagen nuclear PET, X-CT y SPECT.* Dpto. de Física Atómica, Molecular y Nuclear. Universidad Complutense de Madrid, 2008.
7. Price JC, et al. *Noise reduction in PET attenuation correction by maximum likelihood histogram sharpening of attenuation images.* Journal of Nuclear Medicine, 1996. **37**(5): p. 786-794.
8. Chow PL, Rannou FR, Chatziioannou AF. *Attenuation correction for small animal PET tomographs.* Physics in Medicine and Biology, 2005. **50**(8): p. 1837-1850.
9. D'Ambrosio D, et al. *Attenuation correction for small animal PET images: A comparison of two methods.* Computational and Mathematical Methods in Medicine, 2013. **8**(6): p. 1-12.
10. Vicente Torrico E, et al. *Corrección de atenuación de imágenes PET usando datos de TAC en el escáner para animales pequeños Argus PET/CT.* Libro de actas del XXVIII Congreso Anual de la Sociedad Española de Ingeniería Biomédica (CASEIB), 2010: p. 256.
11. Popota FD, et al. *Comparison of the performance evaluation of the MicroPET R4 scanner according to NEMA standards NU 4-2008 and NU 2-2001.* IEEE Transactions on Nuclear Science, 2012. **59**(5): p. 1879-1886.
12. Prasad R, et al. *CT-Based Attenuation Correction on the FLEX Triumph Preclinical PET/CT Scanner.* Nuclear Science, IEEE Transactions on, 2011. **58**(1): p. 66-75.
13. Canadas M, et al. *Performance evaluation for Ga-68 and F-18 of the ARGUS small-animal PET scanner based on the NEMA NU-4 standard.* 2010 IEEE Nuclear Science Symposium Conference Record (NSS/MIC), 2010: p. 3454-3457.
14. *NEMA standards publication NU 4 – 2008. Performance measurements of small animal positron emission tomographs.* National Electrical Manufacturers Association, 2008.
15. Prasad R, Ratib O, Zaidi H. *NEMA NU-04-based performance characteristics of the LabPET-8 (TM) small animal PET scanner.* Physics in Medicine and Biology, 2011. **56**(20): p. 6649-6664.
16. Disselhorst JA, et al. *Image-quality assessment for several positron emitters using the NEMA NU 4-2008 standards in the Siemens Inveon small-animal PET scanner.* Journal of Nuclear Medicine, 2010. **51**(4): p. 610-617.

17. Geworski L, et al. *Recovery correction for quantitation in emission tomography: A feasibility study.* European Journal of Nuclear Medicine, 2000. **27**(2): p. 161-169.
18. Vicente Torrico E. *Caracterización, mejora y diseño de escáneres PET preclínicos.* Dpto. de Física Atómica, Molecular y Nuclear. Universidad Complutense de Madrid, 2013.
19. El Ali HH. *Importance of attenuation correction (AC) for small animal PET imaging diagnostics.* Diagnostics, 2012. **2**: p. 42-51.
20. Goertzen AL, et al. *NEMA NU 4-2008 comparison of preclinical PET imaging systems.* Journal of Nuclear Medicine, 2012. **53**(8): p. 1300-1309.
21. Prasad R, Ratib O, Zaidi H. *Performance evaluation of the FLEX Triumph X-PET scanner using the National Electrical Manufacturers Association NU-4 standards.* Journal of Nuclear Medicine, 2010. **51**(10): p. 1608-1615.
22. Szanda I, et al. *National Electrical Manufacturers Association NU-4 performance evaluation of the PET component of the NanoPET/CT preclinical PET/CT scanner.* Journal of Nuclear Medicine, 2011. **52**(11): p. 1741-1747.
23. Gu Z, et al. *NEMA NU-4 performance evaluation of PETbox4, a high sensitivity dedicated PET preclinical tomograph.* Physics in Medicine and Biology, 2013. **58**(11): p. 3791-3814.